Atmos. Chem. Phys. Discuss., 9, 14361–14451, 2009
www.atmos-chem-phys-discuss.net/9/14361/2009/

Atmospheric Chemistry and Physics Discussions

This discussion paper is/has been under review for the journal *Atmospheric Chemistry and Physics (ACP)*. Please refer to the corresponding final paper in *ACP* if available.

NO_x production by lightning in Hector: first airborne measurements during SCOUT-O3/ACTIVE

H. Huntrieser[1], H. Schlager[1], M. Lichtenstern[1], A. Roiger[1], P. Stock[1], A. Minikin[1], H. Höller[1], K. Schmidt[2], H.-D. Betz[2,3], G. Allen[4], S. Viciani[5], A. Ulanovsky[6], F. Ravegnani[7], and D. Brunner[8]

[1]Institut für Physik der Atmosphäre, Deutsches Zentrum für Luft- und Raumfahrt (DLR), Oberpfaffenhofen, Germany
[2]nowcast GmbH, München, Germany
[3]Physics Department, University of Munich, Germany
[4]School of Earth, Atmospheric & Environmental Sciences, University of Manchester, UK
[5]Istituto Nazionale di Ottica Applicata (CNR-INOA), Firenze, Italy

[6] Central Aerological Observatory, Moscow, Russia
[7] Institute of Atmospheric Sciences and Climate (CNR-ISAC), Bologna, Italy
[8] Laboratory for Air Pollution and Environmental Technology, Empa,
Swiss Federal Laboratories for Materials Testing and Research, Dübendorf, Switzerland

Received: 15 May 2009 – Accepted: 22 June 2009 – Published: 1 July 2009

Correspondence to: H. Huntrieser (heidi.huntrieser@dlr.de)

Published by Copernicus Publications on behalf of the European Geosciences Union.

Abstract

During the SCOUT-O3/ACTIVE field phase in November–December 2005 airborne in situ measurements were performed inside and in the vicinity of thunderstorms over northern Australia with several research aircraft (German *Falcon*, Russian M55 *Geophysica*, and British *Dornier-228*). Here a case study from 19 November is presented in large detail on the basis of airborne trace gas measurements (NO, NO_y, CO, O_3) and stroke measurements from the German LIghtning Location NETwork (LINET), set up in the vicinity of Darwin during the field campaign. The anvil outflow from three different types of thunderstorms was probed by the Falcon aircraft: 1) a continental thunderstorm developing in a tropical airmass near Darwin, 2) a mesoscale convective system (MCS) developing within the tropical maritime continent (Tiwi Islands) known as Hector, and 3) a continental thunderstorm developing in a subtropical airmass ~200 km south of Darwin. *For the first time detailed measurements of NO were performed in the Hector outflow.* The highest NO mixing ratios were observed in Hector with peaks up to 7 nmol mol^{-1} in the main anvil outflow at ~11.5–12.5 km altitude. The mean NO_x (=NO+NO_2) mixing ratios during these penetrations (~100 km width) varied between 2.2 and 2.5 nmol mol^{-1}. The NO_x contribution from the boundary layer (BL), transported upward with the convection, to total anvil-NO_x was found to be minor (<10%). On the basis of Falcon measurements, the mass flux of lightning-produced NO_x (LNO_x) in the well-developed Hector system was estimated to 0.6–0.7 kg(N) s^{-1}. The highest average stroke rate of the probed thunderstorms was observed in the Hector system with 0.2 strokes s^{-1} (here only strokes with peak currents ≥10 kA contributing to LNO_x were considered). The LNO_x mass flux and the stroke rate were combined to estimate the LNO_x production rate in the different thunderstorm types. For a better comparison with other studies, LINET strokes were scaled with Lightning Imaging Sensor (LIS) flashes. The LNO_x production rate per LIS flash was estimated to 4.1–4.8 kg(N) for the well-developed Hector system, and to 5.4 and 1.7 kg(N) for the continental thunderstorms developing in subtropical and tropical airmasses, respectively. If we assume,

ACPD

9, 14361–14451, 2009

that these different types of thunderstorms are typical thunderstorms globally (LIS flash rate ~44 s^{-1}), the annual global LNO_x production rate based on Hector would be ~5.7–6.6 Tg(N) a^{-1} and based on the continental thunderstorms developing in subtropical and tropical airmasses ~7.6 and ~2.4 Tg(N) a^{-1}, respectively. *The latter thunderstorm type produced much less LNO_x per flash compared to the subtropical and Hector thunderstorms, which may be caused by the shorter mean flash component length observed in this storm. It is suggested that the vertical wind shear influences the horizontal extension of the charged layers, which seems to play an important role for the flash lengths that may originate. In addition, the horizontal dimension of the anvil outflow and the cell organisation within the thunderstorm system are probably important parameters influencing flash length and hence LNO_x production per flash.*

1 Introduction

Thunderstorms and lightning are not only spectacular weather phenomena but also have an important influence on the chemical composition of the atmosphere (Dickerson et al., 1987). Most studies indicate that production by lightning is the dominating source of NO_x in the upper troposphere (UT), besides aircraft emissions and downward transport of NO_x-rich air from the stratosphere, at least globally. Here just a brief introduction to LNO_x is given, since details can be found in a recent review article by Schumann and Huntrieser (2007) (=SH07). We found that the best estimate for the global LNO_x source strength was 5±3 Tg(N) a^{-1}. Compared to the major emission sources in the BL from fossil fuel combustion and biomass burning, LNO_x contributes with only 10% to the total NO_x emissions. Due to the longer lifetime of NO_x in the UT compared to the BL, LNO_x has a disproportional large influence on the photochemical production of the greenhouse gas ozone (O_3) (Crutzen, 1970; Chameides and Walker, 1973; Cooper et al., 2006).

Even though the majority of lightning is observed over the continents in the tropics (Christian et al., 2003), studies on LNO_x have mainly been performed in midlatitude

ACPD
9, 14361–14451, 2009

regions (Europe and United States). Up to recently, studies in the tropics were rare (SH07). The field experiment "Tropical Convection, Cirrus and Nitrogen Oxides Experiment" (TROCCINOX) 2004 and 2005 in Brazil was the first in a series of airborne campaigns carried out by European groups in the tropics to investigate LNO_x (Schumann et al., 2004; Huntrieser et al., 2007; SH07; Huntrieser et al., 2008). In the years 2005 and 2006, the "Stratospheric-Climate Links with Emphasis on the Upper Troposphere and Lower Stratosphere" (SCOUT-O3) and "Aerosol and Chemical Transport in Deep Convection" (ACTIVE) campaigns in Australia and the "African Monsoon Multidisciplinary Analyses" (AMMA) campaign in Africa followed (Redelsperger et al., 2006; Allen et al., 2008; Mari et al., 2008; Vaughan et al., 2008; Brunner et al., 2009). More recently in 2007, American groups conducted the "Tropical Composition, Cloud, and Climate Coupling" (TC4) experiment from Costa Rica. Anvils of convective systems primarily off the Pacific coast of Costa Rica and Panama were sampled by research aircraft. As a result of these campaigns, some of the most important global centres of tropical lightning activity have now been investigated in large detail.

Here we present measurements and results obtained from the SCOUT-O3/ACTIVE field experiments performed from the tropical "top end" of Australia, Darwin (−12.4° N, 130.9° E). About 50–100 km north of Darwin over the Tiwi Islands, a very deep convective system develops on a regular basis known as "Hector" (see Fig. 1 and more details in Sect. 2). In the past, a number of field campaigns have been performed in this area, as summarised in Sect. 3. *From this summary it is clear that during the SCOUT-O3/ACTIVE field campaigns for the first time the anvil outflow of Darwin thunderstorm systems was probed systematically and freshly emitted NO was measured*. The general focus of the airborne measurements during SCOUT-O3/ACTIVE was on the chemical composition and transport processes in the tropical tropopause layer (TTL) (e.g. Heyes et al., 2009). It is known that explosive deep convective clouds can penetrate into the TTL. On 19 November 2005, a typical Hector system developed which was investigated in large detail with the German research aircraft *Falcon*. The main focus of the present study is on LNO_x produced by Hector over an isolated tropical island in

ACPD
9, 14361–14451, 2009

comparison to other thunderstorm systems over the mainland, developing in tropical as well as in subtropical airmasses. Our results from the previous field experiment TROCCINOX in Brazil indicate that tropical thunderstorms may produce less LNO_x per flash compared to subtropical thunderstorms (Huntrieser et al., 2008) (=HH08). It was suggested that these differences are related to the different vertical shear of horizontal wind. In the investigated tropical airmasses over Brazil, a much lower wind shear was observed in comparison to the subtropical airmasses (Huntrieser et al., 2007) (=HH07).

Here we present further evidence from the SCOUT-O3/ACTIVE experiments that support this finding. The set up of the airborne trace gas instrumentation and the lightning location network (LINET) during SCOUT-O3/ACTIVE was similar as during TROCCINOX and is described in Sect. 4. The general meteorological situation and a summary of the 19 November flights are given in Sect. 5. The method used to analyse the measurements is introduced in Sect. 4 and discussed in more detail in Sect. 6 together with the results. The Falcon, Geophysica and LINET measurements are combined and scaled with LIS measurements to estimate the LNO_x production rate per LIS flash in different types of thunderstorms (tropical/subtropical/Hector), and *to estimate the global annual LNO_x production rate based on these different thunderstorm types*. The method, which combines the *LNO_x mass flux rate* in the anvil outflow and the *LINET stroke rate*, was already introduced and described in a previous paper (HH08). Finally, reasons for different LNO_x production rates found in different thunderstorm types are discussed (see Sect. 7).

2 Hector

Deep convective clouds in the tropics are essential for the maintenance of the Earth's general circulation. The area north of Australia extending across the Indonesian archipelago to New Guinea is termed the "Maritime Continent" and the "boiler box" of the tropics (Ramage, 1968; Holland and Keenan, 1980). The low-level inflow and

high-level outflow in this area drive the meridional Hadley and equatorial Walker circulation and it is one of the primary regions of global latent heat release (Keenan et al., 1989, 1990). The fast vertical convective transport of BL air to the UT within ~1 h may also affect the composition and chemistry in the TTL (Dessler, 2002).

An especially vigorous deep convective system in this area develops almost on a daily basis during the transition and monsoon break periods (November–March) in response to diurnal heating over the Tiwi Islands north of Darwin. This mesoscale convective system (MCS) is locally known as "Hector" (Keenan et al., 1989, 1990; Danielsen, 1993). The Tiwi Islands consist of two Islands, Bathurst (west) and Melville (east), which are separated by a narrow tidal channel, and extend ~150 km in east-west and ~50 km in north-south direction. The maximum island height is 120 m. Due to its isolated occurrence over these flat islands, Hector is an ideal "atmospheric laboratory" thunderstorm. Numerous numerical and observational studies on Hector have therefore been carried out in the past.

It is known that thunderstorms in the Darwin area belong to the most intense and deepest convective events on Earth, with an especially high frequency of overshooting tops reaching up to 20 km (Keenan et al., 1989; Simpson et al., 1993; Wilson et al., 2001; Liu and Zipser, 2005; Zipser et al., 2006). During the transition period in November–December (=pre-monsoon), Hector systems over the Tiwi Islands are detected on at least 2/3 of the days and the mean lifetime is 2–5 h (Keenan et al., 1990; Beringer et al., 2001). The convection develops in an environment with low to moderate shear, moderate convective available potential energy (CAPE) and high moisture availability. First smaller convective clouds develop in late morning along the coastlines of the Tiwi Islands, strongly influenced by the local sea breeze front (Simpson et al., 1993; Keenan et al., 1994). However, for the development of the vigorous Hector system later in the afternoon, the *merging* of two or more cloud systems and the resulting explosive growth is of fundamental importance, as shown in Fig. 1.

Early numerical simulations by Simpson (1980) and Tao and Simpson (1984, 1989) have suggested that the downdrafts in convection and the associated *cold outflows*

ACPD
9, 14361–14451, 2009

play an important role in the merging process. This gust front outflow may establish "bridge clouds" between two neighbouring cumulonimbi (Cbs). These bridge clouds in the centre of the convergence zone then grow explosively and may become much more intense and taller than previous Cbs (Fig. 2). One of the reasons for unusual strength of the Hector system is that it develops over an isolated heat source, where the interaction between sea breeze fronts from all coastlines and gust fronts from previous convection can contribute to convergence (e.g. Crook et al., 2001). When an evaporatively produced cold pool becomes cooler than the nearby sea breeze front, convection speeds up and displaces the heated island BL even faster than before (Carbone et al., 2000).

Two types of Hector developments have been suggested by Carbone et al. (2000): 1) type A (20%), weaker convection, directly initiated by the collision of inward-penetrating sea breeze fronts from the north and south, when conditions are more stable, 2) type B (80%) is much stronger and is initiated by a multistage (4–5 stages) interaction between sea breeze fronts and gust fronts from earlier convection and develops first near a leeward coast (Fig. 2). The latter finding was confirmed by Beringer et al. (2001) and Brunner et al. (2009) who typically observed Hector developments over the eastern (western) end of the island during westerly (easterly) flow. Many of the strongest Hector systems develop when gust fronts from separate areas over the Bathurst and Melville Islands collide. During the merging stage, one or more extended, long-lived MCS are frequently formed with both convective and stratified cloud areas (Keenan et al., 2000). Common features of Hector squall lines are radar echo tops up to 16–17 km, convective region widths extending 40–50 km, deep anvil depths and an especially high concentration of ice crystals compared to maritime convection (Takahashi and Keenan, 2004). During MCTEX (see Sect. 3) it was observed that in the developing stage of Hector, precipitating convective cells along island sea breezes were dominated by warm rain processes. When the gust front forcing from these storms merged to larger, taller and more intense MCS over the island (Hector), the new system was dominated by mixed-phase precipitation processes.

ACPD
9, 14361–14451, 2009

3 Past field campaigns in the Darwin area and recent results from other studies

In the past, a larger number of field campaigns (partly airborne) were conducted in the Darwin area to investigate tropical deep convection. The "Stratosphere-Troposphere Exchange Project" (STEP) was carried in January–February 1987 during the (wet) monsoon season (Danielsen, 1993; Russell et al., 1993). Highly variable mixing ratios of reactive nitrogen (NO_y) were observed in the UT, which were attributed to the production by lightning (Murphy et al., 1993). Model simulations suggested that this additional source of NO may enhance the ozone production rate in the UT by a factor of 2–3 (Pickering et al., 1993). STEP was coordinated together with the "Australian Monsoon Experiment" (AMEX) (Holland et al., 1986) and the "Equatorial Mesoscale Experiment" (EMEX) (Webster and Houze, 1991). In the pre-phase of these first Darwin campaigns the vigorous development of Hector was visually observed, however it was investigated in detail first during the following-up "Island Thunderstorm Experiment" (ITEX) in November–December 1988 (Keenan et al., 1989; Skinner and Tapper, 1994), *where physical and numerical studies on the generation and evolution of tropical island convection were performed for the pre-monsoon season*.

Dynamical and electrical properties of both tropical continental and maritime storms were investigated during the "Down Under Doppler and Electricity Experiment" (DUNDEE) in 1988/1989/1990 during both pre-monsoon and monsoon seasons (Petersen and Rutledge, 1992; Rutledge et al., 1992; Williams et al., 1992). It was concluded that the large contrast in flash rates between land and ocean systems, by an order of magnitude, is caused by differences in the relative amounts of liquid and ice phase condensate in the mixed-phase region of the storms. The total flash rate of intracloud (IC) and cloud-to-ground (CG) flashes observed in deep continental convection near Darwin was especially high with 20–50 flashes min^{-1}.

In November–December 1995, the "Maritime Continent Thunderstorm Experiment" (MCTEX) followed with the objective to study *cloud electrification processes in Hector*, in particular the coupling between ice phase precipitation and lightning production

ACPD
9, 14361–14451, 2009

(Carbone et al., 2000; Carey and Rutledge, 2000; Keenan et al., 2000; Saito et al., 2001; Takahashi and Keenan, 2004). *For the first time a combination of polarimetric radar and lightning measurements was used*. Some of the results of this study were already discussed in Sect. 2.

In December 2000, phase C of the "Biomass Burning and Lightning Experiment" (BIBLE-C) was performed during the monsoon season (Kondo et al., 2003; Koike et al., 2007). *It was the first aircraft experiment designed to estimate LNO_x production rates in the tropics*, where production is considered to be most intense. During two flights near Darwin, enhanced NO_x and NO_y mixing ratios of up to 1.0–1.6 nmol mol^{-1} (=ppbv) and 1.5–2.0 nmol mol^{-1} (10-s average), respectively, were observed in the UT. Between 11.5 and 14 km altitude the average NO_x mixing ratio was 0.2–0.3 nmol mol^{-1}. The enhancements in NO_x were attributed to intensive lightning events observed several hundred kilometres upstream to the east, over the coast of the Gulf of Carpentaria, active ~10 to 14 h earlier. It was pointed out, that the wide domain with enhanced NO_x mixing ratios (>0.1 nmol mol^{-1}) covering ~500×150 km^2 was unusual for the tropics. It was suggest that LNO_x had a significant influence on UT-NO_x. Lightning data from the ground-based "Global Positioning and Tracking System" (GPATS) and derived column NO production rates were used to estimate the NO production rate per flash. For the two flights, the estimates were 1.9–4.4 and 21–49×10^{25} NO molecules, respectively. These values are near the lower and upper boundaries of the range of 2–40×10^{25} NO molecules per flash given in the review by SH07.

In November 2002, the Australian "Egrett Microphysics Experiment with Radiation, Lidar, and Dynamics in the Tropics" (EMERALD-2) studied the nature of cirrus clouds from the Hector outflow, which extended hundreds of km horizontally and vertically between ~12.2 and ~15.8 km (Whiteway et al., 2004).

Finally, some results from more recent studies concerning convection and LNO_x production over Australia are briefly summarised. Beirle et al. (2004) used NO_2 satellite data from the Global Ozone Monitoring Experiment (GOME) and LIS data over Central Australia to estimate a LNO_x production rate per LIS flash. Their estimate of

100 (30–500) mol or 1.4 (0.4–7) kg (N) per LIS flash would correspond to a global annual production rate of 2.8 (0.8–14) Tg(N) a^{-1}. May and Keenan (2005) and May and Ballinger (2007) used radar information to investigate the differences between thunderstorms developing in monsoon and break regimes. The latter were the most intense, produced a lot of lightning and sometimes even hail, and reached higher altitudes for a given reflectivity threshold. In contrast, monsoon cells were weaker (maritime type) and produced less lightning and more precipitation, especially of stratiform type. Kuleshov et al. (2006) used lightning data from a ground-based detection system and from LIS and the Optical Transient Detector (OTD) to study the spatial distribution and frequency of lightning activity in Australia. In the northern parts of Australia the total flash rate density is in general high with >10 km^{-2} yr^{-1} and the maximum is located at −16° N and 126° E (~35 km^{-2} yr^{-1}). The IC/CG ratio in all parts of Australia varies between 0.75 and 7.7, with a mean around 2 independent of latitude.

4 Data and method

4.1 The SCOUT-O3/ACTIVE campaigns

The coordinated SCOUT-O3 and ACTIVE field campaigns focused on aerosol and chemical transport in deep convection and its effect on the composition of the TTL (Allen et al., 2008; Vaughan et al., 2008; Brunner et al., 2009). SCOUT-O3 Darwin is part of the SCOUT-O3 Integrated Project funded by the European Commission (http://www.ozone-sec.ch.cam.ac.uk/scout_o3/). ACTIVE is a consortium of eight institutions lead by the University of Manchester and funded by the UK Natural Environment Research Council (NERC).

The SCOUT-O3 field phase was carried out from 16 November–5 December 2005 during the so-called pre-monsoon or transition period and about at the same time as the first ACTIVE field phase. The frequent and isolated occurrence of Hector during this period greatly simplifies flight planning. Furthermore, aircraft can rather easily pen-

etrate or circumnavigate these isolated storms over the Tiwi Islands. A second ACTIVE field phase was performed in January 2006 during the monsoon period together with the international "Tropical Warm Pool International Cloud Experiment" (TWP-ICE) (May et al., 2008a, b, 2009).

4.2 Airborne instrumentation: Falcon, Geophysica and Dornier-228

SCOUT-O3 used the Russian research aircraft M55 *Geophysica* and the German *Falcon* of the Deutsches Zentrum für Luft- und Raumfahrt (DLR) for in situ measurements in the anvil outflow region and above. For ACTIVE the "Airborne Research Australia's" (ARA) Grob G520T *Egrett* and the UK Natural Environment Research Council (NERC) *Dornier-228* performed measurements in the anvil outflow and inflow region, respectively. However, here we only report on measurements from the latter aircraft, since only this aircraft performed a flight on 19 November. The airborne instrumentation used for this study and its accuracy are listed in Table 1. The measurements listed below are used to estimate the LNO_x production rate in selected thunderstorm systems (see further details in Sect. 6).

In the present study we mainly concentrate on measurements carried out with the Falcon up to 12.5 km altitude. The aircraft was equipped with instruments to measure NO and NO_y mixing ratios and the photolysis rate $J(NO_2)$. The instrumentation has been used during several DLR field campaigns in the past (e.g. Baehr et al., 2003; Huntrieser et al., 2005; HH07). All instruments are capable of measuring at high temporal resolution ($\leq$1 s) necessary for investigating the small scale structures in the anvil outflow (Huntrieser et al., 1998, 2002; Höller et al., 1999). The NO_2 (and NO_x) mixing ratios are calculated on the basis of the photostationary steady state equation from the measurements of NO, O_3, $J(NO_2)$, pressure and temperature (Volz-Thomas et al., 1996). Since O_3 was not measured on board the Falcon, the vertical O_3 profile from the Geophysica aircraft was used instead. The mean NO/NO_x ratio at an altitude of 10.0–12.5 km during the flight on 19 November 2005 was $\geq$0.9, indicating that errors in the NO_2 estimation have only a small effect on the NO_x estimation in the UT. In addi-

tion, NO, NO_y, CO and O_3 measurements up to ~20 km altitude were obtained from the high-flying Geophysica aircraft (Stefanutti et al., 2004). The latter two trace gases were used as tracers for the rapid upward transport of BL air by convection. Both, the Geophysica and Falcon probed the region around Hector during the selected 19 November mission. The Falcon focused on the anvil outflow region up to 12 km and the Geophysica more on the TTL above. In addition, measurements of CO from the Dornier-228 aircraft on 19 November were used to estimate the contribution of boundary layer NO_x (BL-NO_x) in the anvil outflow.

All three aircraft were equipped with standard meteorological measurement systems to measure position, altitude, temperature, pressure, and in some cases humidity and the 3-dimensional wind vector (u, v, w). All flight altitude values refer to pressure height and UTC (Universal Time Coordinated) time. The time difference between UTC and the Australian Central Standard Time (ACST) in the SCOUT-O3 observation area (Darwin) is −9.5 h (e.g. 16:00 ACST=6:30 UTC).

4.3 Meteorological, lightning, satellite and radar data

For flight planning during the SCOUT-O3/ACTIVE field phases, a variety of model forecasts from the European Centre for Medium-Range Weather Forecasts (ECMWF) and the Bureau of Meteorology's Extended Limited Area Prediction System (TXLAPS) were used. For meteorological analyses, wind fields based on ECMWF data with a horizontal resolution of $1^\circ \times 1^\circ$ are presented in Sect. 5.2.

For the observation of lightning, the six-sensors DLR lightning location network LINET was installed around Darwin as described in Höller et al. (2009). This detection system, operating in the very low frequency/low frequency (VLF/LF) (5–200 kHz) range, has been developed by the University of Munich and described in detail by Betz et al. (2004, 2007, 2009), Schmidt et al. (2004, 2005) and Schmidt (2007). A brief description was recently given by us in HH08 and will therefore not be repeated here. Radiation emitted from both IC and CG sources ("strokes") is detected and the IC emission height is determined. Though these height values are principally representative

for the detected IC discharges, it must be noted that variations of the signal velocity along the path between stroke and sensor, depending on the ground conductivity, may cause some reduction of the given height values (H.-D. Betz, personal communication, University of Munich, 2009). The lightning stations were located in an area extending from −11.3° N to −13.2° N and from 130.4° E to 131.8° E. The average distance to the next closest sensor was ∼90 km. Peak currents down to 1–2 kA were measured in the inner region where the detection efficiency was highest; the so-called LINET centre area covering −12.0 to −13.0° N and 130.5 to 131.5° E. However, a decreasing detection efficiency of strokes with low peak currents with increasing distance from the LINET detection centre has been observed (HH08; Höller et al., 2009). At the current stage, strokes emitted along a lightning channel are considered separately. However, in Sect. 7.1 a small set of strokes within a certain time period (<1 s) and within a closer area (<35 km) was combined to so-called "flash components". For the construction of flash components only strokes with peak currents ≥10 kA were considered for an unbiased comparison between thunderstorms in the inner and outer LINET detection region (see details in HH08). Since similar LINET arrays were also set up in Brazil and Germany in 2005 and in West-Africa in 2006, the characteristics of thunderstorms systems in these study regions can now directly be compared to Australian systems (Höller et al., 2009).

In addition to LINET data, spaceborne measurements from LIS on board the Tropical Rainfall Measurement Mission (TRMM) satellite (Christian et al., 1999; Thomas et al., 2000; Boccippio et al., 2002, Christian and Petersen, 2005) were used to estimate the total regional flash distribution (sum of CG and IC flashes) over the SCOUT-O3/ACTIVE area. For an overview of system characteristics see http://thunder.msfc.nasa.gov/lis/ and a brief description was already given by us in HH08. Here LIS data for three overpasses of 14 and 17 November and 20 December 2005 were compared with LINET data (see Sect. 6.7). Our LNO_x estimates per LINET stroke were scaled to LNO_x estimates per LIS flash. Global LIS flash statistics can then be used to provide an estimate of the global strength of the LNO_x production rate.

The cloud development over northern Australia was analysed by using infrared (IR) and water vapour (WV) images (see Sect. 5.2) from the Multi-functional Transport Satellite-1 Replacement (MTSAT-1R) and the Geostationary Meteorological Satellite (GMS-5), respectively, operated by the Meteorological Satellite Center (MSC) of the Japanese Meteorological Agency (JMA) (http://mscweb.kishou.go.jp/). MTSAT-1R brightness temperatures (see Minnis et al., 2006) were used together with other satellite and meteorological data to derive the cloud-top height (CTH). The method for these calculations (Visible Infrared Solar-Infrared Split Window Technique=VISST) has been described in detail by Minnis et al. (1995). Furthermore, the cloud development was analysed by using radar reflectivity data obtained from the CPOL radar in Darwin (May et al., 2008b) (see Sect. 6.4).

4.4 Method to estimate the annual global LNO_x production rate

In this section our method used to estimate the annual global LNO_x nitrogen mass production rate G_{LNO_x} (in $Tg\,a^{-1}$) is briefly introduced. For an overview of the different steps, see Fig. 3 which is adopted and slightly modified from HH08. More details are also given later in Sect. 6.

Cloud-model simulations indicate that most LNO_x produced in a thunderstorm is transported into the anvil region (Skamarock et al., 2003; Fehr et al., 2004). If the total LNO_x mass in the anvil region (dependent on the LNO_x mixing ratio and the volume covered by this LNO_x) and the total number of flashes in the thunderstorm that contributed to this LNO_x were known, the LNO_x production rate per flash could be estimated, assuming a constant LNO_x production per flash. Up to now, however, no method exists which can determine the required parameters exactly.

Here the horizontal LNO_x mass flux F_{LNO_x} (in nitrogen mass per time, $g\,s^{-1}$) is first calculated from measurements during each anvil penetration according to Chameides

ACPD
9, 14361–14451, 2009

et al. (1987):

$$F_{\mathrm{LNO_x}} = \chi_{\mathrm{LNO_x}} \cdot \frac{M_N}{M_{\mathrm{air}}} \cdot \rho_a (V_a - V_s) \cdot \Delta x \cdot \Delta z \quad (1)$$

where $\chi_{\mathrm{LNO_x}}$ is the mean NO_x volume mixing ratio produced by lightning (mol mol^{-1}), M_N and M_{air} are the molar masses of nitrogen (14 g mol^{-1}) and air (29 g mol^{-1}), respectively, ρ_a is the air density (g m^{-3}) calculated from measured temperature and pressure in the anvil, and $V_a - V_s$ is the difference between the wind vectors in the anvil outflow and at the steering level. In general, the wind at the steering level (~700 hPa) determines the mean motion of a thunderstorm cell (Keenan and Carbone, 1992), but this parameter is not available from the airborne measurements since this region was not probed specifically. Instead, the storm motion (V_s) was determined from the spatial LINET stroke evolution based on horizontal stroke distributions with a high temporal resolution of 10 min. The last term $\Delta x \cdot \Delta z$ is the area (m^2) of the vertical cross-section perpendicular to the wind direction in the anvil outflow. The parameters in Eq. (1), except Δx and Δz, were calculated directly from Falcon measurements by averaging the measured data over the time period when the anvil was penetrated.

For the estimate of the LNO_x production rate $P_{\mathrm{LNO_x}}$ (nitrogen mass per stroke, in g stroke^{-1}) in a thunderstorm, the horizontal LNO_x mass flux $F_{\mathrm{LNO_x}}$ (g s^{-1}) is then divided by the total (IC+CG) contributing LINET stroke rate R_{LINET} (strokes s^{-1}) according to HH08:

$$P_{\mathrm{LNO_x}} = \frac{F_{\mathrm{LNO_x}}}{R_{\mathrm{LINET}}} \quad (2)$$

For comparison with other published results, the $P_{\mathrm{LNO_x}}$ estimates per LINET stroke in Eq. (2) are scaled to $P_{\mathrm{LNO_x}}$ estimates per LIS flash. Finally, it is multiplied with the number of LIS flashes occurring globally, 44±5 flashes s^{-1} according to Christian and Petersen (2005), to achieve the annual global LNO_x nitrogen mass production rate $G_{\mathrm{LNO_x}}$ (in Tg a^{-1}).

5 Observations during SCOUT-O3/ACTIVE

5.1 General meteorological situation

The SCOUT-O3 field phase was carried out between mid November and beginning of December during the pre-monsoon period, when the intertropical convergence zone (ITCZ) is located north of Darwin and the main flow is from the SE off the continent. Later in December, the monsoon (or wet season) starts when the ITCZ moves south of Darwin. The main flow is then from the WNW from maritime regions. Holland (1986) defined the monsoon (break-period) in Darwin to coincidence with the onset and existence of westerly (easterly) flow at 850 hPa. The break period (from monsoon) is similar to the pre-monsoon period that occurs at the end of the dry season before the austral summer monsoon. In the pre-monsoon period (mid-November–mid-December), convection in the Darwin area is dominated by isolated vigorous storms, including the development of Hector MCSs over the Tiwi Islands north of Darwin (Sect. 2). In comparison, during the monsoon period convection is more widespread and less intense.

The large-scale tropical circulation in the Australian/Asian region from November 2005 to April 2006 has been summarised by Shaik and Cleland (2006). A detailed meteorological SCOUT-O3/ACTIVE roadmap has recently been given by Brunner et al. (2009) and partly also by Allen et al. (2008, 2009), Vaughan et al. (2008) and Höller et al. (2009). For this reason just a brief summary is given here.

During the SCOUT-O3 field phase, highly variable conditions regarding wind direction and velocity in the BL and free troposphere were present as described by Brunner et al. (2009) and shown in Fig. 4. During the first and last part of the campaign, weak easterly flow dominated at most levels and the ITCZ (subtropical jet stream) was located far to the north (south) of Darwin, typical for the pre-monsoon period. Due to these weak winds in the UT, the anvils spread in all directions. However, in the middle of the field phase (about 19–27 November) strong westerly winds dominated in the free troposphere, though slightly weaker ones dominated in the BL. This situation was caused by a pronounced Rossby wave breaking activity and unusually strong north-

ward undulation of the southern hemispheric subtropical jet stream (Allen at al., 2009; Brunner et al., 2009). Due to these strong westerly winds in the UT, the anvils spread preferably to the east during this period.

5.2 Flight summary of 19 November 2005

On the selected day in this study, 19 November 2005, three aircraft performed measurements over the Tiwi Islands. For a brief description of these flights and their overall scope, see Vaughan et al. (2008) and Brunner et al. (2009). The Dornier-228 mainly investigated the Hector inflow region over the Tiwi Islands between the BL and up to 3.4 km (04:32–08:22 UTC). A joint flight was performed with the Falcon (03:38–07:34 UTC) and the Geophysica (03:20–08:07 UTC) in the UT and TTL region, respectively. In addition to the investigation of Hector, the latter two aircraft flew long north-south transects, as the trajectory forecasts indicated different airmass origins (tropical/subtropical) north and south of Darwin (see Fig. 21 by Brunner et al., 2009). This sharp transition zone between moist airmasses around Darwin and further north, and drier airmasses 200–300 km south of Darwin is also clearly visible in the WV satellite image from 05:33 UTC (Fig. 5). In this image, also three thunderstorm systems investigated by the aircraft in the different airmasses are highlighted as "1a", "2a", and "3a". Single penetrations of these thunderstorms by the Falcon are described later in more detail and numbered further (e.g. 2a_II=second penetration of thunderstorm 2a). A series of cloud top height images from 02:33–07:33 UTC indicates the temporal development of the convection during the mission flights (Fig. 6a–f). Superimposed are the flight tracks from the Falcon and Geophysica aircraft.

Falcon measurements (Fig. 7a–b) indicate that the wind direction in the BL varied between NW and SW and the wind velocity was week (2–6 m s^{-1}). At the steering level (~700 hPa), the wind varied between W and SW and was still rather weak. In the middle and upper troposphere, the main wind direction was from the W. The wind velocity increased with altitude to ~20 m s^{-1} at 10–12 km altitude about 250 km south of Darwin at the southern turning point 131.5° E and −15.1° N, which was passed twice (Fig. 6b

ACPD
9, 14361–14451, 2009

and e, and Fig. 7a–b at ∼15 000 and 25 500 s). The wind velocity then decreased with increasing latitude to ∼5 m s^{-1} at 10–12 km altitude at the northern turning points 131.5° E and −9.8°/−8.4° N (Fig. 6c–d, and Fig. 7a–b at ∼18 000 and 21 500 s). Consequently, thunderstorms developed under largely variable conditions in terms of shear, which makes this day especially interesting for our studies concerning LNO_x production as mentioned in the introduction. The strong horizontal N–S wind velocity gradient in the UT was caused by the presence of the southern hemispheric *subtropical jet*, which was located unusually close to Darwin on the 19 November as mentioned before (Fig. 8).

At noon local time (LT) (02:30 UTC), first thunderclouds were initiated by the sea breeze front along the southwestern coastline of the Bathurst Island, and along the northwestern and eastern coastlines of the Melville Island (Fig. 6a). The spatial and temporal distribution of LINET strokes presented later in Fig. 9c, confirms this development (see "anvil_2a_west" and "anvil_2a_east"). One hour later, at 13:00 LT (03:30 UTC), these clouds had moved inland, but still three separate convective areas were visible in the satellite image (Fig. 6b). The lightning activity in the western cell over Bathurst Island peaked around 03:20 UTC (∼200 strokes with ≥10 kA in 5 min) (Fig. 10b). About 40 min later, the pre-existing convection and their cold pools merged to a large Hector MCS, located over the western and central part of the Melville Island (Figs. 6c and 9c). Just before 14:00 LT (04:20 UTC), lightning activity in Hector peaked with almost 400 strokes (≥10 kA) in 5 min (Fig. 10b). In the next hours the system slowly dissipated and a huge anvil spread out over the Tiwi Islands and to the east (Figs. 6d–f). Lightning activity decayed until 15:30 LT (06:00 UTC) (Fig. 10b).

After take-off, the Falcon and Geophysica aircraft first headed south to the southern turning point (Fig. 6b). During the Geophysica ascent between −13.1° and −13.4° N, the outflow from a convective cell close to Darwin was penetrated at ∼10–11.5 km. On the way back from the southern turning point, the same outflow labelled "1a_I" was penetrated by the Falcon at 10.7 km (04:36:06–04:38:09 UTC), see Figs. 6c, 7a–b, and 9b. Both aircraft were then directed to the Tiwi Islands, where thunderclouds

initiated by the sea breeze front along the coastline merged to a Hector system. The outflow was advected to the east, however probably mainly the aged outflow from the first smaller thunderclouds, labelled "2a_x" (pre-Hector), was penetrated by the Falcon at 10.7 km (04:45:14–04:47:45 UTC), see Fig. 9c. In Fig. 7a, a twin peak in the NO_x mixing ratio is visible where the penetration of anvil 2a_x is indicated. For the calculations according to Eq. (1), only the first peak was considered since only this one was related to the anvil labelled as "2a_west" in Fig. 9c. The main outflow from Hector was probably located above the Falcon flight level, as discussed in Sect. 6.4. Thereafter, the Falcon headed further north to −9.8° N. About half an hour later, when the lightning activity in Hector started to decay, its outflow was penetrated twice, labelled "2a_I" and "2a_II", by the Falcon at 11.3 km (05:15:50–05:22:20 UTC) and at 11.5–11.9 km (05:27:14–05:35:50 UTC), respectively, see Fig. 9c. Both aircraft then headed to the northernmost turning point, as indicated in Fig. 6d. On the way back, the Falcon aircraft penetrated the Hector outflow once more, labelled "2a_III", at 11.9 km (06:24:37–06:32:42 UTC); see Fig. 6e and Fig. 9c. Before landing, both aircraft headed to the southern turning point again and the Falcon penetrated a third anvil outflow once, labelled "3a_I", on the way back to Darwin during descent between 11.0 and 9.5 km (07:04:38–07:09:10 UTC); see Fig. 6e and Fig. 9d. The Geophysica aircraft mainly flew above all convective outflow (∼17.0–18.5 km), since it focused more on the region of the cold-point tropopause. The cold point tropopause was located at ∼17 km, coinciding with a strong increase in static stability and in the ozone mixing ratio, as discussed later in Sect. 6.4. The three regions, where the penetrated anvils on 19 November occurred (Darwin, Tiwi Islands and a region ∼200 km south of Darwin), are typical regions over northern Australia where the average annual flash density is elevated as shown in Fig. 3 by Kuleshov et al. (2006).

For the evaluation of the penetration height in relation to the cloud top height (CTH), mean ($\pm\sigma$) and median CTH height values are listed in Table 2. Note that the maximum and minimum retrieved CTHs are only 15.9 and 4.0 km, respectively, since the retrieval algorithm tries to avoid errors associated with thermal inversions at the tropopause and

ACPD
9, 14361–14451, 2009

boundary layer. As a result, the maximum CTHs are likely underestimated in particular for the deep overshooting Hector system. The detailed maps in Fig. 6a–f indicate a similar mean CTH for anvil 1a and 3a of 11.3 km and 11.4 km, respectively. For the different penetrations of anvil 2a (Hector) the mean CTH values were partly higher and ranged from 12.7 to 14.1 km. The Falcon aircraft penetrated all anvils downstream, to the east of the cells, whereto the main outflow was advected (Fig. 6a–f). The anvils 1a and 3a were penetrated about 0.6–1.0 km and the well-developed anvil 2a (I–III) about 1.1–1.4 km below the mean CTH. These penetrations were performed well within the anvil outflow layer. However, the first thunderstorm penetration over the Tiwi Islands (2a_x) was performed distinctly below the mean CTH (about 3.4 km) and probably too low to be representative for the main outflow.

The NO and NO_y mixing ratios were distinctly enhanced by a few nmol mol^{-1} during the anvil penetrations (~30–100 km) compared to the background which contained less than 0.1 nmol mol^{-1} NO (Fig. 7b). The high ratio of NO to NO_y (~0.6–0.8) found in the selected anvils indicates that NO was emitted recently and most likely by lightning, as discussed in Sect. 6.2–6.3 and 6.5. The NO_x mixing ratios in the investigated anvils outflows reached a peak value of 7.4 nmol mol^{-1} in Hector (Fig. 7a). For the selected anvil penetrations, the mean NO_x mixing ratios were estimated to ~0.5–2.5 nmol mol^{-1} (Fig. 7a). Coinciding with an increase in NO_x, the wind velocity frequently increased briefly at the anvil edges, but in general decreased inside the anvil outflow compared to the background (Fig. 7a).

Furthermore, in Fig. 7b we also included CN concentrations, since such measurements are rare in anvil outflow region. The particle number concentration (CN>5 nm) was strongly enhanced in the outflow by a factor of ~10 (up to 10 000 particles cm^{-3} at standard temperature and pressure) compared to the background and the BL, except in the aged outflow from anvil 2a_III (Fig. 7b). In agreement with our results, Twohy et al. (2002) found that CN concentrations may be enhanced by more than an order of magnitude within a thunderstorm anvil compared to outside. The nucleation of new particles may be induced by the oxidation of aerosol precursor trace gases transported

ACPD
9, 14361–14451, 2009

into the anvil region from the BL (e.g. Raes et al., 2000), possibly also favoured by relatively low pre-existing surface area (not measured in this study). Due to the lack of further aerosol measurements, our CN observations will not be discussed here in more detail.

6 Estimate of the LNO_x production rate per flash and per year

In this section the measurements in the selected anvils of 19 November 2005 are discussed in more detail and the resulting annual global LNO_x nitrogen mass production rate G_{LNO_x} is estimated. The values needed for the calculations according to Eq. (1) and Eq. (2) are estimated below and listed in Tables 3–5. First, the spatial and temporal distributions of LINET strokes are presented and discussed in Sect. 6.1. These distributions are then used in Sect. 6.2 to associate the individual anvil-NO_x enhancements to corresponding LINET strokes and representative stroke frequencies. The contribution of BL-NO_x to measured anvil-NO_x is estimated in Sect. 6.3. For the calculation of the horizontal LNO_x mass flux rate, the mean depth of the anvil outflow is estimated in Sect. 6.4. The representativeness of the different anvil penetrations according to the measurements is discussed in Sect. 6.5. The horizontal LNO_x mass flux rate out of the anvils is calculated by means of estimated LNO_x mixing ratios and horizontal outflow wind velocities from the flights combined with the size of the vertical cross-section of the anvils (Sect. 6.6). LNO_x nitrogen mass flux rates ($g\,s^{-1}$) and LINET stroke rates (strokes s^{-1}) are then combined to estimate the production rate of LNO_x (in g of nitrogen mass or number of NO_x molecules) per LINET stroke and per LIS flash (Sect. 6.7). Finally, the annual global LNO_x nitrogen mass production rate G_{LNO_x} in $Tg\,a^{-1}$ is estimated.

ACPD
9, 14361–14451, 2009

6.1 Spatial and temporal LINET stroke distributions

On 19 November, convective cells with lightning developed in the late morning along the coastlines preferable east of Darwin and over the Tiwi Islands. In the afternoon, thunderstorms also developed along the coastline southwest of Darwin. The spatial distribution of LINET strokes with peak currents ≥1 kA between 00:00 and 08:00 UTC is shown in Fig. 9a together with the Falcon flight track and measured NO_x mixing ratios. The Hector system over the Tiwi Islands was the strongest storm development in this area and another strong convective system developed ∼100 km south of Darwin. The thunderstorm systems of interest, as described in Sect. 5.2, are labelled 1a, 2a, and 3a, and zoomed in on Fig. 9b–d. All anvil penetrations are characterised by enhanced NO_x mixing ratios close to areas with lightning activity along the flight track, as indicated in Fig. 9a–d. The movement of the systems and the wind direction in the anvil outflow region are indicated with arrows. The latter controls the transport of LNO_x out of the anvils. In the Darwin area and over the Tiwi Islands, the thunderstorms moved to the east. Further south of Darwin, the systems moved more to the north, perpendicular to the UT westerly wind direction.

The temporal distributions of LINET stroke rates in the selected thunderstorms 1a, 2a, and 3a are presented in Fig. 10a–c. For an adequate comparison of the stroke rates in these storms, it was necessary to restrict comparisons to higher stroke peak currents (≥10 kA). These were observed with about the same detection efficiency, independent of their location within the LINET network, as mentioned in Sect. 4.3. The storms of 19 November were mainly in a lightning decaying stage during the aircraft passage, as indicated by the penetration labels in Fig. 10a–c below the time scale. The highest stroke rates were observed in Hector around 04:20 UTC with almost 400 strokes (≥10 kA) per 5 min (Fig. 10b). For comparison, the highest stroke rates observed during TROCCINOX in a subtropical and in tropical thunderstorms (HH08) are superimposed with ∼80 and 40 strokes per 5 min., respectively. These latter values are distinctly lower (factor ∼5–10) compared to Hector stroke rates. The stroke rates in the other SCOUT-O3

ACPD
9, 14361–14451, 2009

thunderstorms 1a and 3a reached up to 180 and 150 strokes per 5 min, respectively (Fig. 10a and c). The lightning activity in the Hector MCS system lasted long, from 02:00–06:00 UTC. In comparison, in the single cell thunderstorm 1a it lasted only ∼1 h. During the lifetime of thunderstorm complex 3a, several new cells developed east of the decaying cells (multicell organisation). The average lifetime of the lightning activity in one cell was ∼1 h, but for the whole thunderstorm complex 3a the activity spread over at least 4 h (04:00–08:00 UTC).

For comparison with other values of the total flash rate in this area, as given in Sect. 3, the high stroke rate observed in Hector ∼400 strokes (≥10 kA) per 5 min was converted into flashes min^{-1}. On average 2–3 strokes per LINET flash were observed, which give 27–40 flashes min^{-1}. These values are well within the range of 20–50 flashes min^{-1} observed in the past during the DUNDEE experiment (Rutledge et al., 1992).

6.2 Contribution from observed LINET strokes to measured anvil-NO_x and resulting stroke rates

For the estimate of the LNO_x production rate per stroke, it is important to know which of the registered LINET strokes contributed to the estimated LNO_x enhancement in the anvil outflow. This is a very difficult task which might be best performed by using cloud-scale modelling. For several TROCCINOX and SCOUT-O3/ACTIVE cases cloud-resolving model simulations are in preparation, but not ready yet (K. Pickering, personal communication, NASA Goddard, 2009). Here we use a rough approximation to estimate the number of LINET strokes contributing to LNO_x. Comparisons between this method of advecting strokes with the ambient wind measured by the aircraft and lightning tracer simulations with a Lagrangian particle dispersion model (FLEXPART) in HH08 indicated that this method can be used if the major fraction of the lightning activity takes place in the upper part of the cloud. Previous cloud-model simulations have indicated that most LNO_x produced in a thunderstorm is transported into the anvil region (Skamarock et al., 2003; Fehr et al., 2004). We assume that LNO_x produced in

overshooting cloud tops, as shown later in Sect. 6.4 for the Hector system, descends and is mainly advected out of the cloud in the main anvil outflow located distinctly below the cloud tops.

Here first the mean ambient wind velocity during 4 min before and after the selected anvil penetrations was determined together with its standard deviation (σ). The whole lifecycle of the stroke activity until the anvil penetration was then divided into 30-min intervals. For each of these intervals it was determined which of the strokes, located upstream of the penetration, could be advected with the mean ambient wind velocity $\pm\sigma$ to the location of the penetration. The mean ambient wind velocities ($\pm\sigma$), the temporal and spatial window of considered strokes, the possible number of strokes contributing to the estimated LNO_x enhancement in the anvil outflow, the mean stroke rates, peak currents and stroke heights for the selected thunderstorm penetrations are listed in Table 3 and partly divided into two data sets: 1.) all peak currents $\geq$1 kA and 2.) only peak currents $\geq$10 kA.

The advection of LINET strokes with the mean ambient wind is probably faster than in reality, since the time for the vertical transport in the cloud was not considered and the horizontal wind velocity in the anvil itself is on average lower than outside (compare mean ambient wind velocities in Table 3 with the wind velocities during the single anvil penetrations in Fig. 7a). Therefore, the advection with the mean ambient wind must be considered as an upper limit for the transport velocity. The mean ambient wind velocities varied between 9 and 12 m s^{-1} for anvil 1a and 2a. In comparison, the wind velocity was distinctly higher for anvil 3a with 18 m s^{-1} located closer to the subtropical jet. However, for the latter thunderstorm, the mean stroke rate (if all peak currents are considered) was lowest of all selected thunderstorms. This is partly caused by the decreasing detection efficiency of strokes with low peak currents with increasing distance from the LINET detection centre. The elevated mean and minimum peak current values of 11.0 and 3.4 kA, respectively (all peak currents considered), for thunderstorm 3a compared to the other selected thunderstorms also indicate that the detection efficiency was reduced.

ACPD
9, 14361–14451, 2009

The mean height of IC strokes was 10.8–11.1 km for the first convective systems (1a and 2a_x) that developed on 19 November. In the well-developed Hector system (2a_I-III) the mean IC stroke height was distinctly higher and located at 12.7–12.8 km. For thunderstorm 3a, IC stroke heights are not available due to the large distance from the LINET detection centre. The mean peak current (for strokes with ≥10 kA) was highest for thunderstorm 2a_x with 22.5 kA. In comparison, for the other thunderstorms 1a, 2a_I–III, and 3a the mean peak current was rather similar with values between 19.1 and 20.3 kA. Based on strokes with peak currents ≥10 kA, the final mean LINET stroke rate contributing to LNO_x was estimated (see last column in Table 3 and also listed in Table 4), which is considered to be a comparable parameter between the different convective systems. The mean stroke rate (for peak currents ≥10 kA) was lowest in the first developing systems 1a and 2a_x with 0.09 and 0.04 strokes s^{-1}, respectively. In the well-developed Hector system (2a_I–III) the mean stroke rate increased to 0.22–0.24 strokes s^{-1}. For thunderstorm 3a, a lower rate of 0.13 strokes s^{-1} was estimated. These values can be compared to distinctly lower mean LINET stroke rates estimated during TROCCINOX, with values between 0.05 and 0.06 strokes s^{-1} for selected tropical thunderstorms and as low as 0.025 strokes s^{-1} for a subtropical thunderstorm (HH08).

For each of the anvil penetrations, the width Δx of the LNO_x plume perpendicular to the wind direction was estimated from the horizontal extension of enhanced anvil-NO_x and the LINET stroke distribution in Fig. 9b–d. This value is needed for further calculations according to Eq. (1). The Δx values obtained are ~35, ~30, ~85–95 and ~60 km for anvil 1a, 2a_x, 2a_I–III and 3a, respectively as listed in Table 4.

6.3 Contribution of boundary layer (BL)-NO_x to anvil-NO_x

The NO_x mixing ratio measured in the anvil outflow is mainly a mixture of LNO_x and NO_x transported upward from the BL with convection (BL-NO_x). In our previous studies (Huntrieser et al., 2002; HH08), the BL contribution to the NO_x mixing ratio in the anvil was derived from the correlation between NO_x and CO mixing ratios in the BL and in

the anvil. It is assumed, that BL air is transported upwards rapidly within strong, well-developed updrafts by the convection, with little ambient mixing and without chemical loss of NO_x and CO. However, during the SCOUT-O3 field phase in Darwin, the Falcon payload did unfortunately not include CO or any other suitable BL tracer. Therefore, we use a combination of trace gas measurements from the Falcon, Geophysica and Dornier-228 aircraft to estimate the BL-NO_x contribution in the anvil outflow region.

The vertical NO_x profile obtained from the Falcon measurements on 19 November reach only down to 3.1 km and no BL-NO_x information is available. During the whole SCOUT-O3 field phase, Falcon measurements of NO_x in the BL are only available from a single flight on 16 November 2005 (Fig. 11a). The mean ($\pm\sigma$) BL-NO_x mixing ratio up to 1 km altitude during this flight was 0.040 ± 0.002 nmol mol^{-1}, which is very low and indicates a very clean BL. The wind direction mainly varied between 180 and 360°. On 19 November it is very likely that the BL-NO_x mixing ratio was similar low or even lower, since maritime airmasses from the west were advected to Darwin. Furthermore, fire maps derived from Moderate Resolution Imaging Spectroradiometer (MODIS) satellite data (Giglio et al., 2003; Davies et al., 2004) indicate that the fire activity in the Darwin area decreased in the period 17–26 November (not shown here, see http://rapidfire.sci.gsfc.nasa.gov/firemaps/). Measurements of CO with the high-flying Geophysica for the entire SCOUT-O3 field phase (Fig. 11b) also indicate that CO was only slightly enhanced in the anvil outflow region at ~10–14 km due to transport from the BL, compared to the region below 10 km. Below 4 km no measurements are available. The mean CO mixing ratios for all SCOUT-O3 flights mainly vary between 70 and 80 nmol mol^{-1} throughout the middle and upper troposphere. In comparison, during TROCCINOX, where the BL was slightly more polluted, the vertical CO profiles showed a distinct C-shape between the BL and UT (HH07). Despite these indications of a minor contribution of BL-NO_x to anvil-NO_x during SCOUT-O3, an upper possible threshold is determined next.

On 19 November, the Falcon measurements indicate that the NO_x mixing ratio between 5 and 3 km altitude increased from 0.03 to 0.08 nmol mol^{-1} (Fig. 12). The

Dornier-228 measurements suggest that CO mixing ratios on average was rather constant between the BL and 3.4 km with 90–100 nmol mol^{-1} (red line) over the region between Darwin and Tiwi Islands. However, some elevated layers at 0.8 and 1.3–1.7 km are visible (black lines) resulting from very small local fires over the Tiwi Islands (Fig. 12). Due to the constant CO mixing ratios on average, we use the NO_x gradient between 5 and 3 km to estimate NO_x in 1 km (BL). The extrapolation is indicated in Fig. 12. It is assumed that the NO_x mixing ratio between 5 and 3 km is increasing due to the decreasing age of NO_x emissions observed towards the BL. With this method a value of ~0.13 nmol mol^{-1} BL-NO_x in 1 km is determined (compare to 90 nmol mol^{-1} CO in 1 km observed by the Dornier-228). This extrapolation is in accordance with the mean increase of the NO_x mixing ratio observed by the Egrett aircraft between 3 and 1 km (also factor 1.6 increase) during other flights in November (A. Volz-Thomas, personal communication, Forschungszentrum Jülich, 2009)

For the selected anvil penetrations of 19 November listed in Table 4, average LNO_x volume mixing ratios χ_{LNO_x} were determined by subtraction of the maximum BL-NO_x contribution (0.13 nmol mol^{-1}) from the mean anvil-NO_x values. Since no further information is available, we here assume that the BL-NO_x contribution was the same for all selected anvils due to the predominately westerly, maritime winds. The mean values for anvil-NO_x ranged between 0.5–2.5 nmol mol^{-1}, as mentioned in Sect. 5.2. As a result, χ_{LNO_x} values from 0.4 to 2.4 nmol mol^{-1} were obtained, as listed in Table 4. These values are distinctly higher compared to TROCCINOX, where χ_{LNO_x} values ranged from 0.1 to 1.1 nmol mol^{-1} (HH08).

Overall, the contribution of BL-NO_x to anvil-NO_x in the selected thunderstorms of 19 November, except anvil 2a_x, was less than 10%. This range is distinctly lower than the average contribution found in European thunderstorms with 25 to 40% (Huntrieser et al., 1998, 2002) and slightly lower than found during TROCCINOX with 10 to 20% (HH08). In the investigated SCOUT-O3 thunderstorms (expect anvil 2a_x), the contribution from LNO_x clearly dominated the anvil-NO_x budget by more than 90%.

ACPD
9, 14361–14451, 2009

6.4 Estimate of the mean depth of the anvil outflow

The mean depth of the anvil outflow Δz is needed as next parameter for estimating the horizontal LNO_x mass flux in Eq. (1). It has been proposed by Folkins et al. (2002) and Folkins and Martin (2005) that the level of maximum anvil outflow and convective detrainment of ozone-poor air from the BL is located where minimum ozone mixing ratios are observed. The vertical O_3 profile obtained from the Geophysica aircraft on 19 November indicates that the main anvil outflow, characterised by especially low O_3 mixing ratios, almost as low as in the BL, was located between 10 and 14 km altitude (Fig. 11c). The selected anvil penetrations at 10 to 12 km (Table 4) were therefore mainly carried out in the lower part and centre of the main anvil outflow.

To estimate the vertical dimensions Δz of the selected anvil outflows (Table 4), a combination of different airborne measurements from the Falcon and Geophysica including vertical profiles of temperature (T), potential temperature (Θ), wind velocity, O_3, CO, and NO mixing ratios was used. The anvil outflow is characterized by a small change in the slope of the T and Θ gradients at the bottom and top of the outflow layer. The wind velocity in the anvil outflow often differs from the ambient wind velocity. However, both a wind increase and decrease can be observed depending on the ambient wind conditions and where the anvil outflow was penetrated. The O_3 and CO mixing ratios in the anvil outflow typically "mirror" the conditions in the BL (Huntrieser et al., 2002). As mentioned earlier, O_3 mixing ratios were corresponding low in the outflow (<40 nmol mol^{-1}), while CO mixing ratios were slightly enhanced by ~5–10 nmol mol^{-1} (Fig. 11b). CO mixing ratios in the BL varied on a daily basis depending on the biomass burning activity (Vaughan et al., 2008). However, on average the mean CO vertical profile from SCOUT-O3 gives no indications of a strong influence from biomass burning emissions in the anvil outflow. Unfortunately, on 19 November a gap in the CO measurements is present in the anvil outflow region between 11.5 and 15 km altitude.

As described in Sect. 5.2, the outflow from anvil 1a was sampled by the Geophysica shortly after takeoff during its ascent towards the south. Unfortunately, no NO measure-

ACPD
9, 14361–14451, 2009

ments were available at this time. However, a distinct decrease in O_3 mixing ratios was observed at 10.2 km (at −13.1° N near anvil 1a) and the constant low O_3 values (35–40 nmol mol^{-1}) continued up to 11.5 km (at −13.4° N, Fig. 13a). These low O_3 mixing ratios indicate a direct upward transport of O_3-poor BL airmasses (30–35 nmol mol^{-1}). The CO mixing ratios in this layer were rather low with ∼75 nmol mol^{-1} (Fig. 13a) indicating no significant contribution from biomass burning emissions in the BL. The wind velocity measured on the Geophysica aircraft indicates a maximum velocity at 10.4 km of 15 m s^{-1}, at the bottom of the anvil outflow, which decreased down to 8 m s^{-1} in the main anvil outflow at 10.5–11.0 km (Fig. 13b). Thereafter, in the upper part of the anvil outflow, the wind velocity increased again to 14 m s^{-1} at 11.8 km. Furthermore, the vertical T and Θ profiles indicate a small change in the gradient at 10.5 and 11.8 km (Fig. 13c–d). This layer was also more unstable than the ambient air below and above this layer. Based on these observations, we assume that the mean depth of the outflow from anvil 1a reached from 10.4–11.8 km and Δz is ∼1.4 km (Table 4).

The Falcon penetrated anvil 1a at 10.7 km, which is in the centre of the main anvil outflow (10.5–11.0 km) as indicated by the low wind velocities and ozone mixing ratios measured before by the Geophysica in this outflow. Additional information is also available from the CPOL radar in Darwin. The vertical radar reflectivity cross section of anvil 1a along the ambient wind direction also indicates that the main outflow was roughly located between 10 and 12 km (Fig. 15a and e). Therefore, we can assume that this penetration, performed when the lightning activity just had decayed (Fig. 10a), is well representative for the conditions in the outflow of anvil 1a.

In comparison, it is more difficult to estimate the vertical extension of the outflow from the Hector pre-storms over the Tiwi Islands labelled anvil 2a_x (04:45:13–04:50:57 UTC), since no nearby ascent or descent is available. However, a time sequence of radar information from the CPOL radar in Darwin is available, as shown in Fig. 15b–d and f–h for the time period 04:00 to 05:00 UTC with focus on the Tiwi Islands. The vertical radar reflectivity cross section of anvil 2a_x along the ambient wind direction indicates that the main anvil outflow was roughly located between 11

and 14 km. Yet, the highest overshooting cloud tops reached up to the cold point tropopause at 17 km, however, there was no significant outflow from these very high altitudes. During the Geophysica ascent, about 1 h before the Hector pre-storm penetration by the Falcon, a second layer with low ozone mixing ratios (25–40 nmol mol^{-1}) was observed between 11.5 and 13.8 km (minimum at 12.0 km) (Fig. 13a). The vertical profile of the wind velocity indicates that this layer reached up to 14.0 km (Fig. 13b). Furthermore, the vertical T and Θ profiles indicate a well-mixed layer between 11.8 and 14.0 km (Fig. 13c–d). The Geophysica ascent was located far away from the anvil outflow, about 150 km to the south, and we may assume that the bottom of the outflow layer was lower closer to the convective cell centre. The rather low NO_x mixing ratios measured by the Falcon aircraft at 10.7 km during the penetration of anvil 2a_x (Table 4), indicate that this penetration was probably performed below the main outflow, as also discussed in Sect. 5.2 based on cloud top height analyses. The first penetration of the well-developed Hector system 2a_I was performed later at 11.3 km, where NO_x mixing ratios were well enhanced (Fig. 7a). We therefore assume that the anvil outflow of anvil 2a_x was located between 11.2 km and 14.0 km, and Δz is ~2.8 km, which is about twice as deep as anvil 1a (Table 4).

For the penetrations of the well-developed Hector system (anvil 2a_I and 2a_II), the same outflow depth was assumed since no closer measurements are available (Table 4). The last penetration of the Hector system (anvil 2a_III) was performed about 1 h after the anvil 2a_II penetration. The measurements during the Geophysica descent, about 100 km south of the Tiwi Islands and 1 h after the last Hector anvil penetration 2a_III, were analysed for the outflow depth. The Figs. 6a–f and 11a–d indicate that the aged outflow from Hector spread over a wide area well beyond the Tiwi Islands. During the Geophysica descent, the vertical T and Θ profiles during indicate a small change in the gradient at 14.2 km and slightly decreasing ozone mixing ratios (from ~30 to ~20 nmol mol^{-1}) below this level down to 11.0 km where a further change in the T and Θ gradient is observed (Fig. 14a and c–d). The anvil 2a_III depth Δz was therefore estimated to ~3.2 km (Table 4). The minimum ozone mixing ratios were observed be-

ACPD
9, 14361–14451, 2009

tween 11.5 and 12.5 km, indicating the level of maximum anvil outflow and convective detrainment of ozone-poor air from the BL. This was also the level where the Falcon penetrated the Hector outflow (11.9 km). The vertical profiles of wind velocity and NO mixing ratios indicate local maxima in this layer due to the strong outflow (Fig. 14a–b). Based on these observations, we may assume that the conditions measured by the Falcon in the outflow of anvil 2a_III at 11.9 km are well-representative for the outflow region. However, since the measurements were performed almost 1 h after the lightning activity decayed (Fig. 10b), the outflow was already aged and not as fresh as during the anvil penetrations 2a_I and 2a_II.

During the Falcon descent into the outflow of anvil 3a between −14.8° N and −14.3° N (Fig. 6e) on its way heading back north to Darwin, NO_x (Fig. 7a) started to increase at 11.0 km (top of the anvil outflow), coinciding with a maximum in wind velocity of 21 m s^{-1} (Fig. 14b). During the descent within the anvil, the wind velocity decreased to a minimum value of 14 m s^{-1} at ∼10.5 km. The wind velocity then increased again to 22 m s^{-1} at 9.5 km, where the Falcon left the anvil outflow at its northern boundary. Yet, this was probably not the bottom of the anvil outflow. Slightly north of anvil 3a (−14.0° N), the Falcon continued the descent and penetrated another anvil outflow that reached down to 8.5 km. This anvil outflow signature is again clearly visible in the wind velocity profile with a wind velocity minimum of 11 m s^{-1} at 8.7 km. The Geophysica aircraft was flying well above this anvil outflow. First during the spiralling Geophysica descent at 07:35–07:44 UTC, distinctly north of the anvil 3a complex (−12.8° N to −12.5° N), the same kind of signatures in the wind velocity were observed. However, the wind minima were more spread and located at 8.5 and 11.0 km. The wind maximum in-between was located at 10.0–10.5 km (Fig. 14b). This signature coincided with a small change in the T and Θ gradient at 8.5 and 11.0 km and a layer with rather constant O_3 mixing ratios in the range of 35–40 nmol mol^{-1} (Fig. 14a and c–d). These O_3 mixing ratios were, however, slightly elevated compared to the Hector outflow located above. Furthermore, a small increase in CO mixing ratios (66–72 nmol mol^{-1}) indicating BL-transport coincided. NO increased with altitude in this outflow layer, indicating

ACPD
9, 14361–14451, 2009

that most NO was produced in the upper part. We assume that the outflow of anvil 3a reached down to 8.5 km. The Geophysica measurements also indicate that the lower level anvil outflow was located between 8.5 and 11.0 km, and Δz was therefore estimated to ~2.5 km (Table 4). Unfortunately, no measurements from the CPOL radar in Darwin were available for this case (out of radar range). Though the distance from the convective cell was larger than during most other selected anvil penetrations and the outflow was slightly more aged (Figs. 9d and 10c), the conditions in the anvil 3a outflow were assumed to be fairly representative since the horizontal transport velocity was also higher.

6.5 Representativeness of the anvil penetrations

Overall, the estimated mean depths of the selected anvil outflows varied between ~1–3 km, which agrees rather well with previous lidar and infrared radiometry observations of anvil depths (~1–2 km) in the Darwin area (Platt et al., 1984). The measurements by Platt et al. (1984) showed that the anvils spread out at altitudes between 7 and 16 km. Our observations during SCOUT-O3 indicate low O_3 mixing ratios at similar altitudes between 9 and 16 km (Fig. 11c). The level of maximum outflow from tropical convective storms is in general located at 12–14 km (Folkins, 2002), where the equivalent potential temperature (Θ_e) is almost the same as at the top of the BL (Highwood and Hoskins, 1998; Folkins et al., 2000). Therefore, this is the maximum altitude that an air parcel from the BL can reach by undiluted, non-overshooting ascent (Folkins et al., 1999). For the computation of Θ_e for a water-saturation pseudo-adiabatic process, the formula developed by Bolton (1980) was used for Falcon data (see also HH07). An extrapolation of the vertical Θ_e profile from 19 November indicates that the temperature at the top of the BL (~1 km) of ~354 K is reached again in the UT at 12.0 to 12.5 km (Fig. 16). Furthermore, on 19 November 2005 the level of maximum outflow, coinciding with the level of minimum O_3 mixing ratios, was located at 11.5 to 12.5 km (Figs. 13a and 14a) and partly covered during the anvil penetrations by the Falcon aircraft. The layer above this O_3 minimum (maximum outflow), up to the cold-point tropopause, is known as the

TTL (Folkins et al., 1999). The mean heights of IC strokes given in Table 3 indicate that the major IC lightning activity was located between 10.8 and 12.8 km, which is in the vicinity of the maximum outflow level. Therefore, we can assume that most of the anvil penetrations carried out by the Falcon aircraft covered the main anvil outflow and the major LNO_x outflow.

For the final calculations it is also important to know if the selected anvils were penetrated in a comparable and representative way. The anvil penetrations listed in Table 4 provide only snapshots of the conditions at a certain level of the cloud at a certain time. These are, however, the only measurements available. It has to be investigated how representative these anvil penetrations are for the average anvil conditions and some important estimates are listed in Table 6. The NO/NO_y ratio gives information on how fresh/aged the emissions were. The overall high ratio of NO to NO_y (~0.6–0.8) found in the selected anvils indicates that NO was emitted recently and most likely by lightning. Most of the measurements were carried out in the decaying stage of the lightning activity (except for anvil 2a_x), however, less than 1 h after lightning decay (Fig. 10a–c). Estimates based on Table 3 indicate that the largest fraction of LNO_x measured during the selected anvil penetrations was produced within the last 2 h before the penetrations (Table 6). All measurements were carried out downstream, in this case east of the main lightning activity (Fig. 9a–d). The distance to the main lightning activity varied between 10 and 90 km (Table 6). At this horizontal distance from the main centre of lightning activity we can assume that the anvil outflow was well accumulated in a certain vertical level. The vertical distance between the aircraft and the mean cloud top height was similar during most anvil penetrations and varied between 0.6 and 1.4 km (except for anvil 2a_x), as already discussed in Sect. 5.2. Except for anvil 2a_x, all selected anvil penetrations were therefore performed well within the main anvil outflow layer.

6.6 Estimate of the horizontal LNO_x mass flux

Based on the parameters estimated in the previous sections and summarised in Table 4, the horizontal LNO_xmass flux F_{LNO_x} (in nitrogen mass per time, g s^{-1}) was calcu-

lated according to Eq. (1) for the selected anvil penetrations. The F_{LNO_x} values ranged between 30 and 694 g s^{-1} and the highest ones were estimated for the well-developed Hector system. The upper range of the values is much higher than estimated for thunderstorms during TROCCINOX, where the same method gave values in the range of 48–178 g s^{-1} (HH08). The fluxes given in Table 4 can be divided by the molar mass for nitrogen and the area of the vertical cross-section ($\Delta x \cdot \Delta z$) to estimate a flux in units of mol m^{-2} s^{-1}. For the selected SCOUT-O3 thunderstorms, these fluxes vary between 2.6 and 20.8×10^{-8} mol m^{-2} s^{-1}. This is a distinctly wider range than found for TROCCINOX thunderstorms with values between 3.3 and 7.1×10^{-8} mol m^{-2} s^{-1}. However, due to the small number of thunderstorms selected, it is not known how representative these values are. The values can also be compared to nitrogen mass fluxes simulated by Barth et al. (2007), who ran different cloud-scale models and achieved 2.7–13.0×10^{-8} mol m^{-2} s^{-1}, and to Barthe et al. (2007), who simulated 6×10^{-8} mol m^{-2} s^{-1} on average in the anvil outflow of a STERAO storm.

The parameters listed in Table 4 have large uncertainties. The relative maximum error of the F_{LNO_x} estimate was therefore calculated, defined as the sum of the single relative errors. The uncertainty for χ_{LNO_x} is given by the standard deviation (on average ~60% of the mean value); for V_a the standard deviations listed in Table 5 indicate an uncertainty of ~20% and for V_s the uncertainty is ~1 m s^{-1} corresponding to ~20%; for Δx and Δz the uncertainties were ~5–10 km and ~0.5–1 km, respectively, corresponding to uncertainties up to ~30% and ~70%. Summing up these uncertainties, the relative maximum error of the F_{LNO_x} estimate is ~200%.

6.7 Estimate of the LNO_x production rate per stroke and per year

For the estimate of the LNO_x production rate P_{LNO_x} (nitrogen mass per stroke, in g stroke^{-1}), the horizontal LNO_x mass flux F_{LNO_x} (g s^{-1}) is divided by the LINET stroke rate R_{LINET} (strokes s^{-1}) according to Eq. (2). P_{LNO_x} estimates for the selected anvil penetrations resulted in values ranging from ~1.1 kg stroke^{-1} for the continental thun-

derstorm 1a, developing in a tropical airmass, and up to ~3.4 kg stroke^{-1} for the continental thunderstorm 3a, developing in a subtropical airmass (Table 4). The well-developed Hector system 2a produced up to ~3.0 kg stroke^{-1}. These results suggest that the Hector system and the continental thunderstorm developing in a subtropical airmass produced more LNO_x per LINET stroke (factor ~3) than the continental thunderstorm developing in a tropical airmass. Possible reasons for these differences will be discussed in more detail in Sect. 7.

For comparison with other published results, the P_{LNO_x} estimates per LINET stroke were scaled to P_{LNO_x} estimates per LIS flash. We are aware of the fact that a LINET stroke is not directly comparable to a LIS flash. Here we only use this LINET stroke – LIS flash relationship for scaling purposes. During and after the SCOUT-O3 field phase, especially two TRMM satellite overpasses of 14 November (10:52:09–10:53:41 UTC) and of 20 December (07:03:54–07:05:54 UTC) provided a sufficient large set of coincident LIS flash observations within the LINET domain with the highest detection efficiency. Lightning activity in the LINET centre area and close-by, covering totally −11.5 to −12.5° N and 130.4 to 132.6° E, was suitable for comparison. During this first (second) selected overpass overall 19 (56) LIS flashes and 33 (96) LINET strokes with peak currents ≥10 kA were registered in this area. For the selected time period, Fig. 17a–b show the horizontal distributions of all available LINET strokes and LIS flashes for the area where lightning occurred. For the P_{LNO_x} estimate, only stronger LINET strokes with peak currents ≥10 kA are considered as mentioned before in Sect. 6.2. The LIS detection efficiency at night (0.93) was taken into account for the LIS overpasses. This implies a LINET/LIS ratio of about (33/19)×0.93=1.6 and (96/56)×0.93=1.6 for the two overpasses respectively, considering only LINET strokes with peak currents ≥10 kA.

By means of this ratio, the mean values for P_{LNO_x} per LIS flash for the continental thunderstorm 1a developing in a tropical airmass is estimated to 1.7 kg, for the well-developed Hector system 2a (expect penetrations x and III) about 4.4 kg, and for the continental thunderstorm 3a developing in a subtropical airmass about 5.4 kg were estimated (Table 4). These values obtained from SCOUT-O3 are well within the range

ACPD
9, 14361–14451, 2009

of values given in a review of previous investigations, where SH07 derived a best-estimate of 3.5 (range 0.5–10) kg of nitrogen per flash. The mean values for P_{LNO_x} per LIS flash during SCOUT-O3 correspond to a total range of 3.4–10.9×10^{25} molecules NO per LIS flash. This range is almost a factor of 2 higher than observed during TROCCINOX (1.9–5.6×10^{25} molecules NO) (HH08).

The different estimates for SCOUT and TROCCINOX thunderstorms may be influenced by the different LINET/LIS ratios obtained. For the selected TROCCINOX case (4 February 2005) a value of only 0.5 LINET strokes per LIS flash was estimated as discussed in HH08, considering only LINET strokes with peak currents ≥10 kA. A second overpass of LIS during TROCCINOX (5 February 2005) was also analysed in the framework of the present study and the same ratio of 0.5 was obtained. Furthermore, a third overpass of LIS during SCOUT-O3 on 17 November 2005 was analysed and the same ratio as estimated for the first two overpasses (1.6), was obtained (not shown). It is not clear why the LINET/LIS ratios during TROCCINOX and SCOUT-O3 are so different. Since the LINET configuration was about the same on the investigated SCOUT-O3 and TROCCINOX days (4–5 stations were active and the average distance to the next closest sensor was ∼80–90 km), we assume that the LINET detection efficiency was similar for peak currents ≥10 kA. However, we speculate that the number of LINET strokes ≥10 kA per LIS flash or the LIS detection efficiency for IC and CG flashes may be different. Results by Höller et al. (2009) indicate an elevated fraction of LINET strokes ≥10 kA and CG strokes for Australia compared to Brazil, which may explain our different LINET/LIS ratios.

The SCOUT-O3 estimates for P_{LNO_x} per LIS flash were finally multiplied with the number of LIS flashes occurring globally, 44 flashes s^{-1}. If we assume that the selected SCOUT-O3 thunderstorms were representative for the globe, the implied *mean* global LNO_x production rate G_{LNO_x} based on these three thunderstorm types, tropical airmass over continent, tropical maritime continent (Hector) and subtropical airmass over continent, would be 2.4, 6.2 and 7.6 Tg a^{-1}, respectively (Table 4). For the estimate of these mean values, the two less representative anvil penetrations 2a_x and 2a_III were not

considered (therefore in brackets). In support to our findings from TROCCINOX, the results from SCOUT-O3 also imply a distinct difference for P_{LNO_x} between continental thunderstorms in tropical and subtropical airmasses (here factor ~3). The values obtained for SCOUT-O3 are partly higher than the estimates for tropical and subtropical thunderstorms over Brazil (HH08). The individual estimates for the single thunderstorm penetrations listed in Table 4, however, indicate that a wide range of values and large uncertainties can be obtained for G_{LNO_x}, depending on where (horizontally and vertically) and when (fresh or aged LNO_x) the anvil was penetrated.

Finally, the relative maximum errors of the P_{LNO_x} and G_{LNO_x} estimates (Table 4) were calculated. The uncertainty for R_{LINET} was estimated from the ratio between total strokes occurring in the cell and the number of strokes considering to have contributed to LNO_x (uncertainty range 30–60%). From the estimates for F_{LNO_x} ~200% and R_{LINET} ~60%, the relative maximum error of the P_{LNO_x} estimate for LINET strokes was ~260%. For the P_{LNO_x} estimate for LIS flashes, it was assumed that the uncertainty in the conversion of LINET strokes (≥10 kA) to LIS flashes was ~30% (depending on which LIS detection efficiency was used: day or night). This gives a relative maximum error of ~290%. For the G_{LNO_x} estimate, the uncertainty in the global LIS flash rate was given with ~10%, which gives a final relative maximum error of ~300%. Considering this relative maximum error, G_{LNO_x} values listed in Table 4 may range up to ~30 Tg a^{-1}. This value is slightly higher than the upper range of ~20 Tg a^{-1} given for G_{LNO_x} in previous assessments (e.g. WMO, 1999; SH07).

7 Possible explanations for different LNO_x production rates in different thunderstorm types

Several recent model simulations indicate that different values for the LNO_x production per flash have to be used depending on region. Simulations with the GEOS-CHEM model (Hudman et al., 2007) reveal that upper tropospheric NO_x mixing ratios observed over the eastern United States during ICARTT (July–August 2004) can only be

reproduced if the LNO_x yield in the model is increased by a factor of 4 to be equivalent to the Ott et al. (2009) value of 7 Tg(N) per flash estimated from cloud-resolved modeling of EULINOX and other midlatitude and subtropical storms. For the same model and period Martin et al. (2006) increased northern mid-latitude LNO_x emissions by a factor 4 to fit aircraft observations, while tropical LNO_x emissions remained unchanged. Furthermore, preliminary results from cloud-model simulations by Pickering et al. (2007) suggest that IC flashes in a tropical thunderstorm during TROCCINOX produce less LNO_x (factor 1.6) compared to their previous cloud model results for IC flashes based on midlatitude and subtropical thunderstorms. In this section we try to find explanations for the different LNO_x production rates observed in different thunderstorm types during SCOUT-O3.

7.1 The importance of the "flash component" length and vertical wind shear

In our recent study on Brazilian thunderstorms during TROCCINOX (HH08), some explanations for the different P_{LNO_x} values obtained for tropical and subtropical thunderstorms were discussed in detail. Here we focus on the major finding from TROCCINOX that the "flash component" length seems to play a significant role for P_{LNO_x}. The longer the flash, the more P_{LNO_x} may be produced if a constant production rate per m is assumed.

The strokes registered by LINET are VLF/LF sources along a flash. It is however not known, which parts of the flash emit these sources. To obtain some information about the flash length, single strokes were therefore combined to a "flash component". A "flash component" is defined as a part of the whole flash and is composed of several strokes (on average 3, however sometimes up to 10) within a certain time period (<1 s) and within a closer area (<35 km). The average time period of a flash component was 0.3 s. For the selected thunderstorms in Table 4, first the average *horizontal* flash component length was estimated (for vertical length see Sect. 7.3). A time period of 20 min was analysed for all thunderstorms when the lightning activity, that contributed to LNO_x, peaked (Table 3). For an unbiased comparison between the selected thunderstorms,

only strokes with peak currents ≥10 kA were considered. The mean horizontal flash component lengths were shortest for the continental thunderstorm "1a_I" developing in a tropical airmass and for the pre-Hector system "2a_x" with values around 2.5–2.7 km (Table 4). In the continental thunderstorm "3a_I", developing in a subtropical airmass, the flash component was distinctly longer and reached 4.3 km on average. Similar and even longer mean flash component lengths, up to 5.5 km, were observed in the well-developed Hector system "2a_I-III" over the Tiwi Islands. The spatial distributions of the horizontal flash component lengths in the selected thunderstorms are shown in Fig. 18. In the tropical airmass thunderstorm and in the pre-Hector systems, the flash components are distributed more closely compared to a more widespread distribution in the well-developed Hector system and in the subtropical airmass thunderstorm complex. Interesting is also the increase in flash component length from 2.5 to 5.5 km, when the smaller pre-Hector thunderclouds merged to a huge Hector system.

Our analyses from TROCCINOX suggested that one reason for the longer horizontal flash component lengths in subtropical compared to tropical thunderstorms may be related to the enhanced vertical shear of the horizontal wind due to the proximity of the subtropical jet stream (HH08). *The elevated vertical wind shear observed in subtropical compared to tropical airmass thunderstorms may distribute charged particles in the cloud over longer horizontal distances (see Sect. 7.2) and we suggest thereby generating longer flashes.*

Figure 19a indicates that the LNO_x production rate per LINET stroke (P_{LNO_x}) is well correlated with the vertical wind shear ($V_a - V_s$), not only for the selected TROCCINOX cases but also for the SCOUT-O3 cases. A distinct positive correlation is visible and the correlation coefficient r^2 for SCOUT-O3 (0.63) is slightly higher than for TROCCINOX (0.54). Interestingly, the slope is about the same for SCOUT-O3 and TROCCINOX. Furthermore, the correlation between the mean annual global LNO_x production rate G_{LNO_x} and the vertical wind shear $V_a - V_s$ for the selected SCOUT-O3 and TROCCINOX cases is shown in Fig. 19b. Again a positive correlation is visible and r^2 for SCOUT-O3 is 0.63 compared to 0.54 for TROCCINOX. However, the slope is much steeper

ACPD
9, 14361–14451, 2009

for SCOUT-O3 due to the higher LINET to LIS rate estimated during SCOUT-O3 (1.6) compared to TROCCINOX (0.5). Figure 19c indicates that the width Δx of the anvil outflow perpendicular to the wind direction is also positively correlated with the flash component length for the selected SCOUT-O3 cases (r^2 is 0.69). Possible mechanisms behind these observations are discussed in the next section.

7.2 Impact of vertical wind shear on thunderstorm and lightning development

An MCS is a good example of a thunderstorm type where the vertical wind shear plays a significant role for the development and that has been investigated in large detail in the literature. A typical MCS consists of four regions: the forward anvil, a convective region (leading line) with the main charge layers (negative in ~5–6 km and positive in the UT), a transition zone and the trailing stratiform region with a negative charge layer in the radar bright band layer around 0°C (see Fig. 1 in Carey et al., 2005; Ely et al., 2008). Carey et al. (2005) and Dotzek et al. (2005) also investigated the lightning density in this kind of storms and found that very high frequency (VHF) lightning sources are located in three major regions: in the negative and positive charge layers in the convective region and in the bright band layer in the trailing stratiform region. Trajectory studies showed that ice particles were advected from the upper positive charge layer in the convective region to the lower bright band layer in the rear (descending pathway). Recently, Ely et al. (2008) investigated the pathway of VHF lightning sources and found that the lightning pathway in a MCS typically extended over 50–60 km in the horizontal. In the initial stage, the lightning pathway spread over a relative constant altitude in the UT (see Fig. 6a in Ely et al., 2008). In the mature stage of the MCS, the lightning pathway then descended from 9–10 km down to 4–5 km in the rear (see Fig. 6b–e in Ely et al., 2008). This first explanation and mechanism has been called the "charge advection mechanism" (Rutledge and MacGorman, 1988). In addition, conceptual models of the electrical structure in a mesoscale convective system (MCS) by Stolzenburg et al. (1994) and in a supercell by Wiens et al. (2005) (both storm types related to elevated wind shear) indicate that the charged regions

in the upper part of the cloud may stretch far away from the convective region with precipitation. Recent simulations by Barthe and Pinty (2007) of an ideal supercellular storm case, using a 3-D mesoscale model with an explicit lightning flash scheme, also point in this direction.

A second possibility for the development of longer flashes may be related to the "tilted dipole mechanism" introduced by Pierce (1955), Brook et al. (1982) and Hill (1988): a lateral displacement of upper level charge inside the convective region itself due to the influence from the vertical wind shear. Later, observations by Rutledge and MacGorman (1988) of MCS and by Engholm et al. (1990) of summer as well as winter storms confirmed a tilted deformation of the charge centres in the convective region by the vertical wind shear. More recently, these findings have been discussed by Gilmore and Wicker (2002), and Carey and Buffalo (2007).

Third, we propose that if a thunderstorm complex has a multicell structure (as for 3a_I) or if single thunderclouds merge (as over the Tiwi Islands to form Hector), longer flashes may be initiated between the centres of different thunderclouds (so-called inter-cloud flashes). Therefore, the horizontal size of the anvil outflow and the cell organization within a thunderstorm system also seems to play an important role for the flash component lengths that may develop (as indicated in Fig. 19c). Recently, Kuhlman et al. (2009) reported that the interaction between charge regions in two converging anvils from supercell storms caused distant flash initiation.

Observations during the DUNDEE experiment (Petersen and Rutledge, 1992; Rutledge et al., 1992; Williams et al., 1992) showed that thunderstorms in the Darwin area typically developed in a low-shear environment, which allow the positive charge in the anvil region to remain above the negative charge layer favouring lightning with less horizontal extension. This low-shear environment is typical for the development of tropical thunderstorms, which tend to be especially narrow and short-lived (as shown in Sect. 5). In contrast, it is known that Hector develops in an environment with moderate shear (Sect. 2) and can last several hours (Keenan et al., 1990; Beringer et al., 2001).

Here we propose that the difference in the estimated horizontal flash components

lengths in the selected TROCCINOX and SCOUT-O3 thunderstorms is related to the different vertical wind shear and size of the systems. However, measurements of the *total flash length* supporting this idea have not been performed or published yet to our knowledge. The new generation of three-dimensional lightning mapping systems though indicate that both CG and IC flashes usually have one or more *extensive horizontal branches* inside the parent thunderstorm (Coleman et al., 2008; Kuhlman et al., 2009), which may extend 30–100 km horizontally.

7.3 Frequency distributions of flash component lengths

In the previous section, a distinct difference in horizontal flash component lengths was found for different types of thunderstorms. For the selected SCOUT-O3 thunderstorms, these lengths are investigated here in more detail on the basis of frequency distributions. In Fig. 20a the horizontal flash component length distributions in thunderstorm "1a_l" (continental tropical airmass) and "3a_l" (continental subtropical airmass) are compared. The number of analysed flash components is 113 for 1a_l and 78 for 3a_l. For both cases the most frequent estimated lengths are <1 km. However, several differences are clearly visible. The fraction of very short lengths (<1 km) is distinctly larger in 1a_l (52% of total) compared to 3a_l (32%). These very short flash components are mainly composed of negative IC strokes at 6–7 km altitude. For 1a_l, the number of flash components generally decreases with increasing length, except a smaller maximum at 2–3 km length. This second maximum is shifted to longer lengths for 3a_l, at 3–4 km. In addition, the fractions of 3–8 km and >20 km lengths are much larger for 3a_l compared to 1a_l.

In Fig. 20b the flash component length distributions in "2a_x" (Hector pre-storms) and "2a_l" (mature Hector) are compared. The number of analysed flash components is 54 for 2a_x and 142 for 2a_l. For both cases the most frequent estimated lengths are <1 km. However, several differences are again clearly visible. The fraction of very short lengths (<1 km) is distinctly larger in 2a_x (57% of total) compared to 2a_l (30%). In addition, the fraction of greater lengths 7–32 km is much larger for the well-developed

ACPD
9, 14361–14451, 2009

Hector system compared to the Hector pre-storms. Interestingly, the average duration of the flash components was only slightly longer for the well-developed Hector (0.28 s) compared to the Hector pre-storms (0.25 s).

The same frequency distribution analyses were also performed for the two selected TROCCINOX cases described in HH08 (however based on lightning data from Rede Integrada Nacional de Detecção de Descargas Atmosféricas, RINDAT). The same kind of differences between thunderstorms that developed in low (tropical) and high (subtropical) wind shear environments were visible (not shown). The fraction of very small lengths (<1 km) was more than twice as high for the tropical thunderstorms on 4 February 2005 (43%) compared to the subtropical thunderstorm on 18 February 2005 (17%).

Next, the *vertical* extent of the flash components was also analysed. Here only strokes within 1a_I were analysed, because for this storm the highest detection efficiency for IC and CG strokes of all selected thunderstorms is available. Short flash components, extending over <1 km horizontally, extended on average over 0.1–0.2 km in the vertical (max. ~1 km). These short flash components were mainly composed of negative (and only few ~10% positive) IC strokes at ~6–7 km altitude (~70%) and some at ~12–17 km altitude (~30%). The majority of these flash components (~60%) propagated *upward* with time. In contrast, the longer flash components, extending over ≥1 km horizontally, extended on average in the vertical over ~2 km (max. ~4 km). These flash components were mainly composed of negative (but also ~40% positive) IC strokes at ~6–7 km altitude (~50%) and at ~12–17 km altitude (~50%) and most flash components (~70%) propagated *downward* with time.

We therefore suggest that the reason for the large fraction of very short flash components in thunderstorms that develop in low-shear environments may be related to the configuration of the charged positive layer in the anvil region. We hypothesize that this layer may be less structured and less developed in low-shear environments. For this reason, a large fraction of the negative IC strokes, generated in the negative charge layer at ~6 km, may discharge earlier than in a setting where they reach an upper well-structured charge layer. The longer flash components that develop more

ACPD
9, 14361–14451, 2009

often in thunderstorms with higher shear are frequently positive IC strokes propagating downward from a probably well structured upper positive charge layer. We further suggest that "warm rain processes", known to dominate in the developing stage of Hector (Sect. 2), may play an important role for development of very short flash components. In comparison, in the well-developed Hector system "mixed-phase precipitation processes" dominate (Sect. 2), which may perhaps support the development of longer flashes. The vertical cross sections of radar reflectivity in Fig. 15f–g indicate that elevated radar reflectivities (>40 dBZ) are observed up to 12 km in the well-developed Hector system. In comparison, in the pre-Hector storms and in thunderstorm 1a such elevated radar reflectivities only reach up to 6 km (Fig. 15e–f, right storms in f), which is close to the level of 0°C (melting level). We therefore suggest, that the cold-cloud depth (distance between the melting level and the storm height) and the concentration of ice and graupel particles were probably much larger in the well-developed Hector compared to the other storms, which may initiate lightning over larger distances. The different hypotheses mentioned above will be investigated in future studies in more detail.

8 Summary and conclusions

In this study measurements performed over northern Australia with several research aircraft (German *Falcon*, Russian M55 *Geophysica*, and British *Dornier-228*) during the SCOUT-O3/ACTIVE field phase in November–December 2005 were analysed. A case study from 19 November was presented in large detail on the basis of airborne trace gas measurements (NO, NO_y, CO, and O_3) carried out inside and in the vicinity of thunderstorms, and stroke measurements from the German LINET lightning location network set up around Darwin. The anvil outflow from three different types of thunderstorms was probed by the Falcon aircraft: a short-lived single cell continental thunderstorm developing in a tropical airmass near Darwin (labelled "1a"), a long-lived MCS developing within the tropical maritime continent (Tiwi Islands) known as Hec-

ACPD
9, 14361–14451, 2009

tor ("2a"), and a long-lived multicell continental thunderstorm complex developing in a more subtropical airmass ~200 km south of Darwin ("3a"). *For the first time detailed NO measurements in the Hector outflow were performed.*

The highest NO_x mixing ratios were observed in the Hector system with peaks up to 7 nmol mol^{-1} in the main outflow at ~11.5–12.5 km altitude. This altitude range almost coincides with the mean height of IC stroke sources at 12.7 km. The mean NO_x mixing ratios during the Hector anvil penetrations, extending over 85–95 km perpendicular to the major wind direction, varied between 2.2 and 2.5 nmol mol^{-1}. The NO_x contribution from the BL, transported upward with the convection, to total anvil-NO_x was found to be minor (<10%). On the basis of Falcon measurements, the LNO_x mass flux in the well-developed Hector system was estimated to 0.6–0.7 kg(N) s^{-1}. The highest stroke rate of all selected thunderstorms was also observed in the Hector system with 0.2 strokes s^{-1} (here only LINET strokes with peak currents ≥10 kA contributing to LNO_x were considered for an unbiased comparison with the other thunderstorms).

These results from Falcon and LINET measurements were then combined to estimate the LNO_x production rate in the different types of thunderstorms described above. A rather high production rate was obtained for the well-developed Hector system with 2.6–3.0 kg(N) per LINET stroke (only ≥10 kA considered). The LNO_x production rate was even higher in the thunderstorm complex "3a" with subtropical airmass signatures with 3.4 kg(N), but lower in the thunderstorm "1a" with tropical airmass signatures with 1.1 kg(N) per LINET stroke. For a better comparison with other studies, LINET strokes were scaled with LIS flashes and a factor of 1.6 LINET strokes per LIS flash was estimated. The LNO_x production rate per LIS flash (P_{LNO_x}) was obtained to 4.1–4.8 kg(N) for the well-developed Hector, 5.4 kg(N) for the subtropical airmass thunderstorm complex, and 1.7 kg(N) for the tropical airmass thunderstorm. These values are slightly lower than results from cloud-resolving model simulations of a further Hector case (16 November 2005) performed recently by Huntemann et al. (2009), which gave ~7 kg(N) per flash.

If we assume, that our different types of thunderstorms are typically global thunder-

storms (LIS flash rate ~44 s^{-1}), the annual global LNO_x production rate (G_{LNO_x}) based on Hector (tropical maritime continent) would be ~5.7–6.6 Tg(N) a^{-1} and based on the continental thunderstorms developing in subtropical and tropical airmasses ~7.6 and ~2.4 Tg(N) a^{-1}, respectively. This result indicates, that Hector has a similar high LNO_x production rate as the subtropical airmass thunderstorm. *The range of all G_{LNO_x} values given here ~2.4–7.6 Tg(N) a^{-1} is well within the range of 5±3 Tg(N)a^{-1}, as given in SH07 as best present estimate of the annual global LNO_x production rate.*

Several reasons for the different LNO_x production rates in different thunderstorm types were suggested and discussed, however no major differences in the mean stroke peak currents (range 19.1–22.6 kA for peak currents ≥10 kA) were observed. Instead, the different mean flash lengths obtained seem to be more related to the observed differences. The length was not directly measured but estimated from a combination of several nearby LINET strokes in time and space to a so-called "flash component". The horizontal length of this flash component was about twice as long for Hector (4.2–5.5 km) and the subtropical airmass thunderstorm (4.3 km) compared to the tropical airmass thunderstorm (2.7 km). The fraction of very short flash component lengths (<1 km) was about twice as high for the latter thunderstorm compared to the other two. The major part of these very short flash components was composed of negative IC strokes propagating upward only ~0.1–0.2 km from 6–7 km altitude. The reason for the difference in flash component length between the latter two thunderstorm types seems to be related to the vertical wind shear between the anvil outflow region and the steering level, which was much higher in the outflow region of the subtropical airmass thunderstorm (15 m s^{-1}) compared to the tropical airmass thunderstorm (6 m s^{-1}). A distinct difference in vertical wind shear between tropical and subtropical environments influencing the flash component length was also observed during TROCCINOX (HH08). For the selected SCOUT-O3 thunderstorms it was shown that *the LNO_x production rate per LINET stroke and the annual global LNO_x production rate were positively correlated with the vertical wind shear $V_a - V_s$(r^2=0.6), which seems to be an important*

ACPD
9, 14361–14451, 2009

parameter not considered up to now in studies quantifying LNO_x.

It is known that the wind shear may influence the structure of charged layers in a thunderstorm as discussed in Sect. 7.2. We hypothesize that the lateral displacement of upper level charge in the convective region because of enhanced vertical wind shear, the so-called "tilted dipole mechanism", may cause longer flash lengths. Furthermore, it has been observed that ice particles can be advected from the positive charge layer in the convective region to the bright band layer in the rear stratiform region (descending pathway), the so-called "charge advection mechanism". We suggest that the two mechanisms described above may enhance the average flash length inside a thunderstorm. However, we also hypothesize that longer flashes may originate if flashes connect charge centres of different thunderclouds (inter-cloud flashes), as in the case of the merging Hector system. The vertical wind shear within the well-developed Hector system was distinctly lower than in the subtropical airmass thunderstorm, though the flash component length was about the same. *Both the dimension and the cell organisation within a thunderstorm system seem to play an important role for the flash lengths that may originate. Furthermore, a positive correlation (r^2=0.7) was observed between the flash component length and the horizontal anvil dimension*.

Based on our findings and hypotheses from SCOUT-O3/ACTIVE, we suggest that different estimates for the amount of LNO_x produced per flash are needed for more accurate global LNO_x estimates, taking into account the *vertical wind shear* between anvil outflow region and storm steering level, the *dimension and cell organisation* of the thunderstorm system and furthermore if *warm rain or mixed-phase precipitation processes* are dominating. For future LNO_x parameterisations we recommend the incorporation of these parameters and to use more detailed radar information. *Especially the ice and graupel volume mass seem to be crucial parameters for the flash length that may be generated and produce LNO_x.* Recently, Yoshida et al. (2009) reported on a clear relationship between the cold-cloud depth (distance between the melting level and the storm height) and the flash rate. In addition, we suggest that the cold-cloud width (impacted by the vertical wind shear) is important to take into account because it

affects the flash length and therefore also the total LNO_x production.

Furthermore, for future field campaigns we suggest to use the new generation of three-dimensional lightning location systems that determine the total flash length more precisely (e.g. the French ONERA VHF interferometric mapper or the New Mexico Tech Lightning Mapping Array, LMA) and to use a comprehensive instrumentation on both microphysics and chemistry. In near future, two field campaigns are planned for summer 2009 and 2010 (http://www.vortex2.org/) focusing on the origin, structure, evolution of tornadoes accompanying thunderstorms over the United States. In addition, for summer 2011 the Deep Convective Clouds & Chemistry Experiment (DC3) field campaign is planned over the central and south-eastern parts of the United States (http://utls.tiimes.ucar.edu/science/dc3.html). The objective of DC3 is to quantify the impact of continental, midlatitude convective storm dynamics, multiphase chemistry, lightning, and physics on the transport of chemical constituents to the upper troposphere. It is planned to use several aircraft to probe the inflow and outflow of thunderstorms and the LMA and LINET lightning systems. With such a comprehensive setup, further improvements for the quantification of LNO_x can be expected.

Acknowledgements. The measurements presented here from the Integrated Project SCOUT-O3 were partially funded by the European Commission under the contract (505390-GOCE-CT-2004) and partly by the DLR (Deutsches Zentrum für Luft- und Raumfahrt) and other SCOUT-O3 partners. ACTIVE was supported by NERC Airborne Remote Sensing Facility and the U.S. Natural Environment Research Council (Grant NE/C512688/1). We thank C. Schiller (Forschungszentrum Jülich), R. MacKenzie (Lancaster University), T. Peter (ETH Zürich), and G. Vaughan (University of Manchester) for the coordination of the SCOUT-O3 and ACTIVE field campaigns. We thank the Falcon, Geophysica and Dornier-228 pilots, the engineers and scientists of the flight departments for the excellent support during the field phase and A. Lewis (University of York) for performing the CO measurements on the Dornier-228 aircraft used in this paper. The LINET system was installed in the Darwin area as a joint effort between DLR and the Bureau of Meteorology Research Center (BMRC) which is now part of the Centre for Australian Weather and Climate Research (CAWCR) and by support from the U.S. DOE-ARM (Department of Energy – Atmospheric Radiation Measurement Program) for TWPICE (Tropical Warm Pool International Cloud Experiment). We greatly acknowledge B. Atkinson, A. Noonan

(Bureau of Meteorology), and L. Oswald (DLR) for making the LINET system operations possible, and M. Zich (nowcast GmbH) for the system support. We thank P. May (CAWCR) for providing the C-POL radar data which were of great help for interpreting the airborne data and the lightning evolution. We express our gratitude to the lightning team at MSFC-NASA for the access to the LIS data. ECMWF is acknowledged for permitting access to their data archives. Finally, we thank L. Labrador (University of Manchester) and E. Defer (Observatoire de Paris – LERMA) for helpful discussions on ACTIVE trace gas and LINET lightning measurements, respectively, and N. Dotzek and V. Grewe (DLR) for helpful comments on the manuscript.

References

Allen, G., Vaughan, G., Bower, K. N., et al.: Aerosol and trace-gas measurements in the Darwin area during the wet season, J. Geophys. Res., 113, D06306, doi:10.1029/2007JD008706, 2008.

Allen, G., Vaughan, G., Brunner, D., May, P. T., Heyes, W., Minnis, P., and Ayers, J. K.: Modulation of tropical convection by breaking Rossby waves, Q. J. Roy. Meteorol. Soc., 135, 125–137, 2009.

Baehr, J., Schlager, H., Ziereis, H., Stock, P., van Velthoven, P., Busen, R., Ström, J., and Schumann, U.: Aircraft observations of NO, NO_y, CO, and O_3 in the upper troposphere from 60° N to 60° S – Interhemispheric differences at midlatitudes, Geophys. Res. Lett., 30, 1598, doi:10.1029/2003GL016935, 2003.

Barth, M. C., Kim, S.-W., Wang, C., Pickering, K. E., Ott, L. E., Stenchikov, G., Leriche, M., Cautenet, S., Pinty, J.-P., Barthe, Ch., Mari, C., Helsdon, J. H., Farley, R. D., Fridlind, A. M., Ackerman, A. S., Spiridonov, V., and Telenta, B.: Cloud-scale model intercomparison of chemical constituent transport in deep convection, Atmos. Chem. Phys., 7, 4709–4731, 2007, http://www.atmos-chem-phys.net/7/4709/2007/.

Barthe, C. and Pinty, J.-P.: Simulation of a supercellular storm using a three-dimensional mesoscale model with an explicit lightning flash scheme, J. Geophys. Res., 112, D06210, doi:10.1029/2006JD007484, 2007.

Barthe, C., Pinty, J.-P., and Mari, C.: Lightning-produced NO_x in an explicit electrical scheme

tested in a Stratosphere-Troposphere Experiment: Radiation, Aerosols, and Ozone case study, J. Geophys. Res., 112, D04302, doi:10.1029/2006JD007402, 2007.
Beirle, S., Platt, U., Wenig, M., and Wagner, T.; NO_x production by lightning estimated with GOME, Adv. Space Res., 34, 793–797, 2004.
Beringer, J., Tapper, N. J., and Keenan, T. D.: Evolution of maritime continent thunderstorms under varying meteorological conditions over the Tiwi Islands, Int. J. Climatol., 21, 1021–1036, 2001.
Betz, H.-D., Schmidt, K., Oettinger, W. P., and Wirz, M.: Lightning detection with 3D-discrimination of intracloud and cloud-to-ground discharges, Geophys. Res. Lett., 31, L11108, doi:10.1029/2004GL019821, 2004.
Betz, H.-D., Schmidt, K., Fuchs, B., Oettinger, W. P., and Höller, H.: Cloud lightning: Detection and utilization for total lightning measured in the VLF/LF regime, J. Lightning Res., 2, 1–17, online available at: http://www.jorl.org, 2007.
Betz, H.-D., Schmidt, K., Laroche, P., Blanchet, P., Oettinger, W. P., Defer, E., Dziewit, Z., and Konarski, J.: LINET – An international lightning detection network in Europe, Atmos. Res., 91, 564–573, 2009.
Boccippio, D. J., Koshak, W. J., and Blakeslee, R. J.: Performance assessment of the tropical transient detector and lightning imaging sensor. Part I: Predicted diurnal variability, J. Atmos. Ocean. Tech., 19, 1318–1332, 2002.
Bolton, D.: The computation of equivalent potential temperature, Mon. Weather Rev., 108, 1046–1053, 1980.
Brook, M., Nakano, M., Krehbiel, P., and Takeuti, T: The electrical structure of the Hokuriku winter thunderstorms, J. Geophys. Res., 87, 1207–1215, 1982.
Brunner, D., Siegmund, P., May, P. T., Chappel, L., Schiller, C., Müller, R., Peter, T., Fueglistaler, S., MacKenzie, A. R., Fix, A., Schlager, H., Allen, G., Fjaeraa, A. M., Streibel, M., and Harris, N. R. P.: The SCOUT-O3 Darwin Aircraft Campaign: rationale and meteorology, Atmos. Chem. Phys., 9, 93–117, 2009, http://www.atmos-chem-phys.net/9/93/2009/.
Carbone, R. E., Wilson, J. W., Keenan, T. D., and Hacker, J. M.: Tropical Island convection in the absence of significant topography. Part I: Life cycle of diurnally forced convection, Mon. Weather Rev., 128, 3459–3480, 2000.
Carey, L. D. and Rutledge, S. A.: The relationship between precipitation and lightning in tropical island convection: A C-band polarimetric radar study, Mon. Weather Rev., 128, 2687–2710,

2000.
Carey, L. D., Murphy, M. J., McCormick, T. L., and Demetriades, N. W. S.: Lightning location relative to storm structure in a leading-line, trailing-stratiform mesoscale convective system, J. Geophys. Res., 110, D03105, doi:10.1029/2003JD004371, 2005.
Carey, L. D. and Buffalo, K. M.: Environmental control of cloud-to-ground lightning polarity in severe storms, Mon. Weather Rev., 135, 1327–1353, 2007.
Chameides, W. L. and Walker, J. C. G.: A photochemical theory of tropospheric ozone, J. Geophys. Res., 34, 8751–8758, 1973.
Chameides, W. L., Davis, D. D., Bradshaw, J., Rodgers, M., Sandholm, S., and Bai, D. B.: An estimate of the NO_x production rate in electrified clouds based on NO observations from the GTE/CITE 1 fall 1983 field operation, J. Geophys. Res., 92, 2153–2156, 1987.
Christian, H. J., Blakeslee, R. J., Goodman, S. J., et al.: The Lightning Imaging Sensor, Proceedings of the 11th International Conference on Atmospheric Electricity, Guntersville, Alabama, 7–11 June, 746–749, 1999.
Christian, H. J., Blakeslee, R. J., Boccippio, D. J., et al.: Global frequency and distribution of lightning as observed from space by the Optical Transient Detector, J. Geophys. Res., 108, 4005, doi:10.1029/2002JD002347, 2003.
Christian, H. J. and Petersen, W.: Global lightning activity, Conference on Meteorological Applications of Lightning Data, 85th AMS Annual Meeting, San Diego, CA, 10–12 January, 2005.
Coleman, L. M., Stolzenburg, M., Marshall, T. C., and Stanley, M.: Horizontal lightning propagation, preliminary breakdown, and electric potential in New Mexico thunderstorms, J. Geophys. Res., 113, D09208, doi:10.1029/2007JD009459, 2008.
Cooper, O. R., Stohl, A., Trainer, M., et al.: Large upper tropospheric ozone enhancements above mid-latitude North America during summer: In situ evidence from the IONS and MOZAIC ozone measurement network, J. Geophys. Res., 111, D24S05, doi:10.1029/2006JD007306, 2006.
Crook, N. A.: Understanding Hector: The dynamics of island thunderstorms, Mon. Weather Rev., 129, 1550–1563, 2001.
Crutzen, P. J.: The influence of nitrogen oxides on the atmospheric ozone content, Q. J. Roy. Meteorol. Soc., 96, 320–327, 1970.
Danielsen, E. F.: In situ evidence of rapid, vertical, irreversible transport of lower tropospheric air into the lower tropical stratosphere by convective cloud turrets and by larger-scale up-

welling in tropical cyclones, J. Geophys. Res., 98, 8665–8681, 1993.
Davies, D., Kumar, S., and Descloitres, J.: Global fire monitoring using MODIS near-real-time satellite data, GIM Int., 18(4), 41–43, 2004.
Dessler, A. E.: The effect of deep tropical convection on the tropical tropopause layer, J. Geophys. Res., 107(D3), 4033, doi:10.1029/2001JD000511, 2002.
Dickerson, R. R., Huffman, G. J., Luke, W. T., et al.: Thunderstorms: An important mechanism in the transport of air pollutants, Science, 235, 460–465, 1987.
Dotzek, N., Rabin, R. M., Carey, L. D., MacGorman, D. R., McCormick, T. L., Demetriades, N. W., Murphy, M. J., and Holle, R. L.: Lightning activity related to satellite and radar observations of a mesoscale convective system over Texas on 7–8 April 2002, Atmos. Res., 76, 127–166, 2005.
Ely, B. L., Orville, R. E., Carey, L. D., and Hodapp, C. L.: Evolution of the total lightning structure in a leading-line, trailing-stratiform mesoscale convective system over Houston, Texas, J. Geophys. Res., 113, D08114, doi:10.1029/2007JD008445, 2008.
Engholm, C. D., Williams, E. R., and Dole R. M.: Meteorological and electrical conditions associated with positive cloud-to-ground lightning, Mon. Weather Rev., 118, 470–487, 1990.
Fehr, T., Höller, H., and Huntrieser, H.: Model study on production and transport of lightning-produced NO_x in an EULINOX supercell storm, J. Geophys. Res., 109, D09102, doi:10.1029/2003JD003935, 2004.
Folkins, I., Loewenstein, M., Podolske, J., Oltmans, S. J., and Proffitt, M.: A barrier to vertical mixing at 14 km in the tropics: Evidence from ozonesondes and aircraft measurements, J. Geophys. Res., 104, 22095–22102, 1999.
Folkins, I., Oltmans, S. J., and Thompson, A. M.: Tropical convective outflow and near surface equivalent potential temperatures, Geophys. Res. Lett., 27, 2549–2552, 2000.
Folkins, I.: Origin of lapse rate changes in the upper tropical troposphere, J. Atmos. Sci., 59, 992–1005, 2002.
Folkins, I., Braun, C., Thompson, A. M., and Witte, J.: Tropical ozone as an indicator of deep convection, J. Geophys. Res., 107, 4184, doi:10.1029/2001JD001178, 2002.
Folkins, I. and Martin, R. V.: The vertical structure of tropical convection and its impact on the budgets of water vapor and ozone, J. Atmos. Sci., 62, 1560–1573, 2005.
Giglio, L., Descloitres, J., Justice, C. O., and Kaufman, Y. J.: An enhanced contextual fire detection algorithm for MODIS, Remote Sens. Environ., 87, 273–282, 2003.
Gilmore, M. S. and Wicker, L. J.: Influences of the local environment on supercell cloud-to-

ground lightning, radar characteristics, and severe weather on 2 June 1995, Mon. Weather Rev., 130, 2349–2372, 2002.
Heyes, W. J., Vaughan, G., Allen, G., Volz-Thomas, A., Pätz, H.-W., and Busen, R.: Composition of the TTL over Darwin: local mixing or long-range transport?, Atmos. Chem. Phys. Discuss., 9, 7299–7332, 2009, http://www.atmos-chem-phys-discuss.net/9/7299/2009/.
Highwood, E. J. and Hoskins, B. J.: The tropical tropopause, Q. J. Roy. Meteorol. Soc., 124, 1579–1604, 1998.
Hill, R. D.: Interpretation of bipole patterns in a mesoscale storm, Geophys. Res. Lett., 23, 643–645, 1988.
Holland, G. J.: Interannual variability of the Australian summer monsoon at Darwin: 1952–82, Mon. Weather Rev., 114, 594–604, 1986.
Holland, G. J. and Keenan, T. D.: Diurnal variations of convection over the maritime continent, Mon. Weather Rev., 108, 223–225, 1980.
Holland, G. J., McBride, L., Smith, R. K., Jasper, D. J., and Keenan, T. D.: The BMRC Australian Monsoon Experiment: AMEX, B. Am. Meteorol. Soc., 67, 1466–1472, 1986.
Höller, H., Finke, U., Huntrieser, H., Hagen, M., and Feigl, C.: Lightning produced NO_x (LINOX) - Experimental design and case study results, J. Geophys. Res., 104, 13911–13922, 1999.
Höller, H., Betz, H.-D., Schmidt, K., Calheiros, R. V., May, P., Houngninou, E., and Scialom, G.: Lightning characteristics observed by a VLF/LF lightning detection network (LINET) in Brazil, Australia, Africa and Germany, Atmos. Chem. Phys. Discuss., 9, 6061–6146, 2009, http://www.atmos-chem-phys-discuss.net/9/6061/2009/.
Hudman, R. C., Jacob, D. J., Turquety, S., et al.: Surface and lightning sources of nitrogen oxides in the United States: Magnitudes, chemical evolution, and outflow, J. Geophys. Res., 112, D12S05, doi:10.1029/2006JD007912, 2007.
Huntemann, T., Pickering, K., et al.: Cloud-resolving simulations of Hector during SCOUT-O3/ACTIVE: case 16 November 2005, in preparation, 2009.
Huntrieser, H., Schlager, H., Feigl, C., and Höller, H.: Transport and production of NO_x in electrified thunderstorms: Survey of previous studies and new observations at mid-latitudes, J. Geophys. Res., 103, 28247–28264, 1998.
Huntrieser, H., Feigl, C., Schlager, H., Schröder, F., Gerbig, C., van Velthoven, P., Flatøy, F., Théry, C., Petzold, A., Höller, H., and Schumann, U.: Airborne measurements of NO_x, tracer species and small particles during the European Lightning Nitrogen Oxides Experiment, J.

Geophys. Res., 107(D11), 4113, doi:10.1029/2000JD000209, ACH 5-1–ACH 5-24, 2002.
Huntrieser, H., Heland, J., Schlager, H., et al.: Intercontinental air pollution transport from North America to Europe: Experimental evidence from airborne measurements and surface observations, J. Geophys. Res., 110, D01305, doi:10.1029/2004JD005045, 2005.
Huntrieser, H., Schlager, H., Roiger, A., Lichtenstern, M., Schumann, U., Kurz, C., Brunner, D., Schwierz, C., Richter, A., and Stohl, A.: Lightning-produced NO_x over Brazil during TROCCINOX: airborne measurements in tropical and subtropical thunderstorms and the importance of mesoscale convective systems, Atmos. Chem. Phys., 7, 2987–3013, 2007, http://www.atmos-chem-phys.net/7/2987/2007/.
Huntrieser, H., Schumann, U., Schlager, H., Höller, H., Giez, A., Betz, H.-D., Brunner, D., Forster, C., Pinto Jr., O., and Calheiros, R.: Lightning activity in Brazilian thunderstorms during TROCCINOX: implications for NO_x production, Atmos. Chem. Phys., 8, 921–953, 2008, http://www.atmos-chem-phys.net/8/921/2008/.
Keenan, T. D. and Carbone, R. E.: A preliminary morphology of precipitation systems in tropical northern Australia, Q. J. Roy. Meteorol. Soc., 118, 283–326, 1992.
Keenan, T. D., Manton, M. J., Holland, G. J., and Morton, B. R.: The Island Thunderstorm Experiment (ITEX) –A study of tropical thunderstorms in the Maritime Continent, B. Am. Meteorpl. Soc., 70, 152–159, 1989.
Keenan, T. D., Morton, B. R., Zhang, X. S., and Nyguen, K.: Some characteristics of thunderstorms over Bathurst and Melville Islands near Darwin, Australia, Q. J. Roy. Meteorol. Soc., 116, 1153–1172, 1990.
Keenan, T. D., Ferrier, B., and Simpson, J.: Development and structure of a maritime continent thunderstorm, Meteorol. Atmos. Phys., 53, 185–222, 1994.
Keenan, T. D., Rutledge, S., Carbone, R., et al.: The Maritime Continent Thunderstorm Experiment (MCTEX): Overview and some results, B. Am. Meteorol. Soc., 81, 2433–2455, 2000.
Koike, M., Kondo, Y., Kita, K., et al.: Measurements of reactive nitrogen produced by tropical thunderstorms during BIBLE-C, J. Geophys. Res., 112, D18304, doi:10.1029/2006JD008193, 2007.
Kondo, Y., Ko, M., Koike, M., Kawakami, S., and Ogawa. T.: Preface to special section on Biomass Burning and Lightning Experiment (BIBLE), J. Geophys. Res., 108, D08397, doi:10.1029/2002JD002401, 2003.
Kuhlman, K. M., MacGorman, D. R., Biggerstaff, M. I., and Krehbiel, P. R.: Light-

ning initiation in the anvils of two supercell storms, Geophys. Res. Lett., 36, L07802, doi:10.1029/2008GL036650, 2009.
Kuleshov, Y., Mackerras, D., and Darveniza, M.: Spatial distribution and frequency of lightning activity and lightning flash density maps of Australia, J. Geophys. Res., 111, D19105, doi:10.1029/2005JD006982, 2006.
Liu, C. and Zipser, E. J.: Global distribution of convection penetrating the tropical tropopause, J. Geophys. Res., 110, D23104, doi:10.1029/2005JD006063, 2005.
Mari, C. H., Cailley, G., Corre, L., Saunois, M., Attié, J. L., Thouret, V., and Stohl, A.: Tracing biomass burning plumes from the Southern Hemisphere during the AMMA 2006 wet season experiment, Atmos. Chem. Phys., 8, 3951–3961, 2008, http://www.atmos-chem-phys.net/8/3951/2008/.
Martin, R. V., Sioris, C. E., Chance, K., et al.: Evaluation of space-based constraints on global nitrogen oxide emissions with regional aircraft measurements over and downwind of eastern North America, J. Geophys. Res., 111, D15308, doi:10.1029/2005JD006680, 2006.
May, P. T. and Ballinger, A.: The statistical characteristics of convective cells in a monsoon regime (Darwin, Northern Australia), Mon. Weather Rev., 135, 82–92, 2007.
May, P. T. and Keenan, T. D.: Evaluation of microphysical retrievals from polarimetric radar with wind profiler data, J. Appl. Meteorol., 44, 827–838, 2005.
May, P. T., Mather, J. H., Vaughan, G., and Jakob, C.: Characterizing oceanic convective cloud systems: The Tropical Warm Pool International Cloud Experiment, B. Am. Meteorol. Soc., 89, 153–155, doi:10.1175/BAMS-89-2-153, 2008a.
May, P. T., Mather, J. H., Vaughan, G., Jakob, C., McFarquhar, G. M., Bower, K. N., and Mace, G. G.: The Tropical Warm Pool International Cloud Experiment, B. Am. Meteorol. Soc., 89, 629–645, doi:10.1175/BAMS-89-5-629, 2008b.
May, P. T., Allen, G., Vaughan, G., and Connolly, P.: Aerosol and thermodynamic effects on tropical cloud systems during TWPICE and ACTIVE, Atmos. Chem. Phys., 9, 15–24, 2009, http://www.atmos-chem-phys.net/9/15/2009/.
Minnis, P., Young, D. F., Kratz, D. P., Coakley Jr., J. A., King, M. D., Garber, D. P., Heck, P. W., Mayor, S., and Arduini, R. F.: Cloud Optical Property Retrieval (Subsystem 4.3), Clouds and the Earth's Radiant Energy System (CERES) algorithm theoretical basis document, Volume III: cloud analyses and radiance inversions (Subsystem 4), NASA RP 1376, edited by: CERES Science Team , NASA, 135–176, 1995.
Minnis, P., Nguyen, L., Smith, W. L, et al.: Large-scale cloud properties and radiative fluxes

over Darwin during TWP-ICE, Proc. 16th ARM Sci. Team Mtg., Albuquerque, NM, 27–31 March, online available at: http://www.arm.gov/publications/proceedings/conf16/extended_abs/minnis_p.pdf), 2006.

Murphy, D. M., Fahey, D. W., Proffitt, M. H., Liu, S. C., Chan, K. R., Eubank, C. S., Kawa, S. R., and Kelly, K. K.: Reactive nitrogen and its correlation with ozone in the lower stratosphere and upper troposphere, J. Geophys. Res., 98, 8751–8773, 1993.

Ott, L. E., Pickering, K. E., Stenchikov, G. L., Huntrieser, H., and Schumann, U.: Effects of lightning NO_x production during the July 21 European Lightning Nitrogen Oxides Project storm studied with a three-dimensional cloud-scale chemical transport model, J. Geophys. Res., 112, D05307, doi:10.1029/2006JD007365, 2007.

Ott, L. E., Pickering, K. E., Stenchikov, G. L., Allen, D., DeCaria, A., Ridley, B., Lin, R.-F., Lang, S., Tao, W.-K.: Production of lightning NO_x and its vertical distribution calculated from 3-D cloud-scale chemical transport model simulations, J. Geophys. Res., submitted, 2009.

Petersen, W. A. and Rutledge, S. A.: Some characteristics of cloud-to-ground lightning in tropical northern Australia, J. Geophys. Res., 97, 11553–11560, 1992.

Pickering, K. E., Thompson, A. M., Tao, W.-K., and Kucsera, T. L.: Upper tropospheric ozone production following mesoscale convection during STEP/EMEX, J. Geophys. Res., 98, 8737–8749, 1993.

Pickering, K. E., Huntemann, T., Ott, L., Barth, M., Huntrieser, H., Schlager, H., Schumann, U., Vaughan, G., and Volz-Thomas, A.: Cloud-resolved simulations of lightning-NO_x in observed tropical thunderstorms, European Geosciences Union, General Assembly 2007, Vienna, Austria, 15–20 April 2007, Oral Paper Nr. EGU2007-A-11013, Geophys. Res. Abstracts, 9, 2007.

Pierce, E. T.: The development of lightning discharges, Q. J. Roy. Meteorol. Soc., 81, 229–240, 1955.

Platt, C. M. R., Dilley, A. C., Scott, J. C., Barton, I. J., and Stephens, G. L.: Remote sounding of high clouds. V: Infrared properties and structures of tropical thunderstorm anvils, J. Clim. Appl. Meteorol., 23, 1296–1308, 1984.

Raes, F., van Dingenen, R., Vignati, E., Wilson, J., Putaud, J. P., Seinfeld, J. H., and Adams, P.: Formation and cycling of aerosols in the global troposphere, Atmos. Environ., 34, 4214–4240, 2000.

Ramage, C. S.: Role of a tropical maritime continent in the atmospheric circulation, Mon. Weather Rev., 96, 365–370, 1968.

Redelsperger, J. L., Thorncroft, C. D., Diedhiou, A., Lebel, T., Parker, D. J., and Polcher, J.: African Monsoon Multidisciplinary Analysis: An International Research Project and Field Campaign, B. Am. Meteorol. Soc., 87(12), 1739–1746, doi:10.1175/BAMS-87-12-1739, 2006.

Russell, P. B., Pfister, L., and Selkirk, H. B.: The tropical experiment of the Stratosphere-Troposphere Exchange Project (STEP): Science objectives, operations, and summary findings, J. Geophys. Res., 98, 8563–8589, 1993.

Rutledge, S. A. and MacGorman, D. R.: Cloud-to-ground lightning activity in the 10-11 June 1985 mesoscale convective system observed during the Oklahoma-Kansas PRE-STORM project, Mon. Weather Rev., 116, 1393–1408, 1988.

Rutledge, S. A., Williams, E. R., and Keenan, T. D.: The Down-Under Doppler and Electricity Experiment (DUNDEE): Overview and preliminary results, B. Am. Meteorol. Soc., 73, 3–16, 1992.

Saito, K., Keenan, T., Holland, G., and Puri, K.: Numerical simulation of the diurnal evolution of tropical island convection over the maritime continent, Mon. Weather Rev., 129, 378–400, 2001.

Schmidt, K., Betz, H.-D., Oettinger, W. P., Wirz, M., and Diendorfer, G.: A new lightning detection network in southern Germany, 27th International Conference on Lightning Protection (ICLP), September 2004, Avignon, France, 2004.

Schmidt, K., Betz, H.-D., Oettinger, W. P., Wirz, M., Pinto Jr., O., Naccarato, K. P., Höller, H., Fehr, T., and Held, G.: A comparative analysis of lightning data during the EU-Brazil TROCCINOX/TroCCiBras campaign, VIII International Symposium on Lightning Protection (SIPDA), 21–25 November 2005, São Paulo, Brazil, 2005.

Schmidt, K.: Ortung und Analyse von Blitzentladungen mittels Registrierung von VLF-Atmospherics innerhalb eines Messnetzes, Ph.D. thesis, Ludwig-Maximilians-Universität, Munich, Germany, 2007.

Schumann, U., Huntrieser, H., Schlager, H., Bugliaro, L., Gatzen, C., and Hoeller, H.: Nitrogen Oxides from thunderstorms – Results from experiments over Europe and the Continental Tropics, paper presented at Deutsch-Österreichisch-Schweizerische Meteorologen-Tagung (DACH), Deutsche Meteorologische Gesellschaft, Karlsruhe, Germany, 7–10 September, 2004.

Schumann, U. and Huntrieser, H.: The global lightning-induced nitrogen oxides source, Atmos. Chem. Phys., 7, 3823–3907, 2007,

http://www.atmos-chem-phys.net/7/3823/2007/.
Shaik, H. A. and Cleland, S. J.: The tropical circulation in the Australian/Asian region – November 2005 to April 2006, Aust. Meteorol. Mag., 55, 219–230, 2006.
Simpson, J.: Downdrafts as linkage in dynamic cumulus seeding effects, J. Appl. Meteorol., 19, 477–487, 1980.
Simpson, J., Keenan, T. D., Ferrier, B., Simpson, R. H., and Holland, G. J.: Cumulus mergers in the maritime continent region, Meteorol. Atmos. Phys., 51, 73–99, 1993.
Skamarock, W. C., Dye, J. E., Defer, E., Barth, M. C., Stith, J. L., Ridley, B. A., and Baumann, K.: Observational- and modelling-based budget of lightning-produced NO_x in a continental thunderstorm, J. Geophys. Res., 108, 4305, doi:10.1029/2002JD002163, 2003.
Skinner, T. and Tapper, N.: Preliminary sea breeze studies over Bathurst and Melville Islands, Northern Australia, as part of the Island Thunderstorm Experiment (ITEX), Meteorol. Atmos. Phys., 53, 77–94, 1994.
Stefanutti, L., MacKenzie, A. R., Santacesaria, V., et al.: The APE-THESEO Tropical Campaign: An overview, J. Atmos. Chem., 48, 1–33, 2004.
Stolzenburg, M., Marshall, T. C., Rust, W. D., et al.: Horizontal distribution of electrical and meteorological conditions across the stratiform region of a mesoscale convective system, Mon. Weather Rev., 122, 1777–1797, 1994.
Takahashi, T. and Keenan, T. D.: Hydrometeor mass, number, and space charge distribution in a "Hector" squall line, J. Geophys. Res., 109, D16208, doi:10.1029/2004JD004667, 2004.
Tao, W.-K. and Simpson, J.: Cloud interactions and merging: Numerical simulations, J. Atmos. Sci., 41, 2901–2917, 1984.
Tao, W.-K. and Simpson, J.: A further study of cumulus interactions and mergers: Three-dimensional simulations with trajectory analyses, J. Atmos. Sci., 46, 2974–3004, 1989.
Thomas, R. J., Krehbiel, P. R., Rison, W., Hamlin, T., Boccippio, D. J., Goodman, S. J., and Christian, H. J.: Comparison of ground-based 3–dimensional lightning mapping observations with satellite-based LIS observations in Oklahoma, Geophys. Res. Lett., 27, 1703–1706, 2000.
Twohy, C. H., Clement, C. F., Gandrud, B. W., et al.: Deep convection as a source of new particles in the midlatitude upper troposphere, J. Geophys. Res., 107, 4560, doi:10.1029/2001JD000323, 2002.
Vaughan, G., Schiller, C., MacKenzie, A. R., Bower, K., Peter, T., Schlager, H., Harris, N. R. P., and May, T. P.: SCOUT-O3/ACTIVE High-altitude aircraft measurements around deep

tropical convection, B. Am. Meteorol. Soc., 89, 647–662, 2008.
Volz-Thomas, A., Lerner, A., Pätz, H.-W., Schultz, M., McKenna, D. S., Schmitt, R., Madronich, S., and Röth, E. P.: Airborne measurements of the photolysis frequency of NO_2, J. Geophys. Res., 101, 18613–18627, 1996.
Webster, P. J. and Houze Jr., R. A.: The Equatorial Experiment (EMEX): An overview, B. Am. Meteorol. Soc., 72, 1481–1505, 1991.
Whiteway, J. A., Cook, C., Gallagher, M., et al.: Anatomy of cirrus clouds: Results from the Emerald airborne campaigns, Geophys. Res. Lett., 31, L24102, doi:10.1029/2004GL021201, 2004.
Wiens, K. C., Rutledge, S. A., and Tessendorf, S. A.; The 29 June 2000 supercell observed during STEPS. Part II: Lightning and charge structure, J. Atmos. Sci., 62, 4151–4177, 2005.
Williams, E. R., Rutledge, S. A., Geotis, S. G., Renno, N., Rasmussen, E., and Rickenbach, T.: A radar end electrical study of tropical "hot towers", J. Atmos. Sci., 49, 1386–1395, 1992.
Wilson, J. W., Carbone, R. E., Tuttle, J. D., and Keenan, T. D.: Tropical island convection in the absence of significant topography. Part II: Nowcasting storm evolution, Mon. Weather Rev., 129, 1637–1655, 2001.
WMO: Scientific Assessment of Ozone Depletion: 1998, World Meteorological Organisation, Geneva, Switzerland, 1999.
Yoshida, S., Morimoto, T., Ushio, T., and Kawasaki, Z.: A fifth-power relationship for lightning activity from Tropical Rainfall Measuring Mission satellite observations, J. Geophys. Res., 114, D09104, doi:10.1029/2008JD010370, 2009.
Zipser, E. J., Cecil, D. J., Liu, C., Nesbitt, S. W., and Yorty, D. P.: Where are the most intense thunderstorms on earth?, B. Am. Meteorol. Soc., 87, 1057–1071, 2006.

Table 1. Airborne instrumentation during SCOUT-O3/ACTIVE used for the present study.

Aircraft (maximum altitude, km)	Species	Technique	Averaging Time, s	Horizontal Resolution, m	Accuracy	Principal Investigator
Dornier-228 (3.4 km)	CO	Aerolaser AL5003	1	~80	±1 nmol mol^{-1}	Alastair Lewis, University of York, UK
Falcon (12.5 km)	Wind (u, v, w)	Rosemount flow angle sensor	1	~200	1 m s^{-1} horizontal, 0.3 m s^{-1} vertical	Andreas Giez, DLR, Germany
	Temperature	PT100/Rosemount	1		0.5 K	
	Humidity	Composite of dewpoint mirror/ capacitive sensor/Lyman Alpha absorption instrument	1			
	NO	Chemiluminescence	1		±1 pmol mol^{-1}	Hans Schlager, DLR, Germany
	NO_y		1		±5 pmol mol^{-1}	
	$J(NO_2)$	Filter radiometry			10%	Hans Schlager, DLR, Germany
	Condensation nuclei	CN counter	1		10%	Andreas Minikin, DLR, Germany
Geophysica (20 km)	O_3	FOZAN chemiluminescence	1	~150	±10 nmol mol^{-1}	F. Ravegnani, Consiglio Nazionale delle Richerche (CNR), Bologna, Italy; A. Ulanovski, CAO, Russia
	NO	SIOUX chemiluminescence	1		10%	Hans Schlager, DLR, Germany
	NO_y		1		15%	
	CO	Tunable diode laser spectrometer	4	~600	9%	Silvia Viciani, INOA, Italy

ACPD
9, 14361–14451, 2009

Table 2. Cloud top height (CTH) statistics on 19 November 2005 retrieved from MTSAT-1R brightness temperatures.

Flight and Anvil Penetration	Selected Area, °N/°E	Entry Time of Penetration, UTC	CTH Mean±σ, km	CTH, Median km
191105_1a_I *"Darwin"*	−12.2 to −13.2/ 131.0 to 132.1	04:36	11.3±3.0	12.6
191105_2a_x *"Focus Tiwi"*	−11.5 to −12.0/ 130.5 to 131.5	04:45	14.1±1.5	14.4
191105_2a_I *"Tiwi"*	−11.0 to −12.0/ 130.0 to 132.0	05:16	12.7±2.0	13.2
191105_2a_II	do.	05:27	12.8±1.9	13.3
191105_2a_III	do.	06:25	13.0±1.5	13.2
191105_3a_I *"South of Darwin"*	−14.0 to −15.0/ 129.5 to 131.5	07:05	11.4±2.6	12.4

Table 3. The mean ambient wind velocity ($\pm\sigma$), the temporal and spatial window of considered strokes, the number of strokes contributing to the estimated LNO_x enhancement in the anvil outflow, the mean stroke rates, peak currents and stroke heights for the selected anvil penetrations.

Anvil Penetration	Mean Ambient Wind Velocity $\pm\sigma$, m s^{-1}	Stroke Time Interval, UTC	Start Longitude, °E	End Longitude, °E	Number of LINET Strokes (all kA)	Mean Stroke Rate (all kA), strokes s^{-1}	Mean (Min.) Stroke Peak Current (all kA)[1], kA	Mean Height of IC Strokes, km	Mean Stroke Peak Current (≥10 kA), kA	Mean Stroke Rate (≥10 kA), strokes s^{-1}
191105_1a_I	12±2	03:00–03:30	130.69	131.10	52					
		03:30–04:00	130.95	131.28	6019					
		04:00–04:36:06	131.20	131.50	635					
						1.349	4.4 (1.2)	10.8±3.1	20.3	0.091
191105_2a_x	10±2	02:00–02:30	130.31	130.85	5					
		02:30–03:00	130.53	131.00	60					
		03:00–03:30	130.74	131.14	331					
		03:30–04:00	130.96	131.28	724					
		04:00–04:30	131.18	131.43	2451					
		04:30–04:45:13	131.39	131.50	3					
						0.424	5.7 (1.8)	11.1±4.9	22.5	0.037
191105_2a_I	12±2	02:00–02:30	129.70	130.35	635					
		02:30–03:00	129.95	130.53	1129					
		03:00–03:30	130.20	130.71	4493					
		03:30–04:00	130.45	130.89	3925					
		04:00–04:30	130.70	131.07	7158					
		04:30–05:00	130.96	131.25	10 897					
		05:00–05:15:50	131.21	131.35	359	2.496	5.8 (1.8)	12.8±3.8	19.1	0.235
191105_2a_II	10±3	02:00–02:30	129.63	130.50	635					
		02:30–03:00	129.86	130.62	1809					
		03:00–03:30	130.09	130.75	4542					
		03:30–04:00	130.33	130.87	3911					
		04:00–04:30	130.56	131.00	3944					
		04:30–05:00	130.80	131.13	8724					
		05:00–05:27:14	131.03	131.24	2139					
						2.130	6.1 (1.8)	12.7±3.8	19.7	0.221
191105_2a_III	9±2	02:00–02:30	129.75	130.51	635					
		02:30–03:00	129.95	130.64	1983					
		03:00–03:30	130.15	130.77	4587					
		03:30–04:00	130.35	130.89	3947					
		04:00–04:30	130.55	131.02	4863					
		04:30–05:00	130.74	131.14	9076					
		05:00–05:30	130.94	131.27	2482					
		05:30–06:00	131.14	131.40	116					
		06:00–06:24:37	131.34	131.50	0					
						2.145	6.0 (1.8)	12.7±3.8	19.7	0.218
191105_3a_I	18±2	04:00–04:30	128.98	129.71	0					
		04:30–05:00	129.34	130.00	1153					
		05:00–05:30	129.70	130.29	355					
		05:30–06:00	130.06	130.58	1295					
		06:00–06:30	130.42	130.87	501					
		06:30–07:00	130.78	131.15	141					
		07:00–07:04:38	131.14	131.20	0					
						0.383	11.0 (3.4)	–	19.4	0.126

[1] These values strongly depend on the detection efficiency in the present area. The detection efficiency of strokes with low peak currents is decreasing with increasing distance from the LINET detection centre (see Sects. 4.3 and 6.2).

ACPD
9, 14361–14451, 2009

Table 4. Estimates of horizontal LNO_x mass flux F_{LNO_x}, LINET stroke rate R_{LINET}, LNO_x production rate per LINET stroke and per LIS flash P_{LNO_x}, and global LNO_x production rate per year G_{LNO_x}.

Flight and Anvil Penetration/ tropical (t), subtropical (s) or Hector (H)	Entry and Exit Time (UTC), s	Pressure Altitude, km	Mean χ_{LNO_x}, nmol mol^{-1}	$\lvert V_a - V_s \rvert$[1], m s^{-1}	ρ_a, kg m^{-3}	Δx, km	Δz, km	$F^2_{LNO_x}$, g(N) s^{-1}	R^3_{LINET}, (LINET strokes) s^{-1}	P_{LNO_x}, g(N) (LINET stroke)$^{-1}$	P_{LNO_x}, g(N) (LIS flash)$^{-1}$	G_{LNO_x}, Tg(N) a^{-1}	Mean LINET Flash Component Length, km
191105_1a_I (t)	(<)16 566–16 689	10.7	2.30	6.3	0.36	35	1.4 (10.4–11.8)	123	0.114	1082	1743	2.4	2.67
191105_2a_x (t)	17114–17265	10.7	0.38	5.4	0.36	30	2.8 (11.2–14.0)	30	0.037	810	1295	(1.8)	2.48
	mean tropical[4]											***2.4***	
191105_2a_I (H)	(<)18 950–19 340	11.3	2.41	7.6	0.33	85	2.8 (11.2–14.0)	694	0.235	2955	4758	6.6	5.46
191105_2a_II (H)	19 634–20 150	11.7 (11.5–11.9)	2.03	7.4	0.31	90	2.8 (11.2–14.0)	567	0.221	2563	4127	5.7	4.23
191105_2a_III (H)	23 077–23 562	11.9	2.02	2.8	0.31	95	3.2 (11.0–14.2)	257	0.218	1180	1900	(2.6)	4.24
	mean Hector[4]											***6.2***	
191105_3a_I (s)	(<)25 478–25 750	10.4 (11.0–9.5)	1.04	14.9	0.38	60	2.5 (8.5–11.0)	426	0.126	3384	5449	7.6	4.32
	mean subtropical											***7.6***	
	relative max. error		*~60%*	*~40%*		*~30%*	*~70%*	*~200%*	*~60%*	*~260%*	*~290%*	***~300%***	

[1] Horizontal anvil outflow velocity, calculated from values in Table 5.

[2] The horizontal LNO_x mass flux out of the anvil, see Eq. (1).

[3] Only LINET strokes with peak currents ≥10 kA contributing to LNO_x were considered for an unbiased comparison between anvil 1a and 2a (strokes mainly inside the LINET centre) and anvil 3a (strokes outside the LINET centre).

[4] For the mean values only the most representative penetrations were selected (penetrations in brackets neglected).

ACPD
9, 14361–14451, 2009

Table 5. Measured wind velocity and direction in the anvil outflow and estimated for the steering level[1].

Flight and Anvil Penetration	Measured Wind Direction in Anvil Outflow d_a, °	Measured Wind Velocity in Anvil Outflow V_a, m s^{-1}	Wind Direction at Steering Level[1] d_s, °	Wind Velocity at Steering Level[1] V_s, m s^{-1}
191105_1a_I	284±8	10.9±2.7	300	5.0
191105_2a_x	267±13	9.4±2.4	294	5.6
191105_2a_I	259±10	13.1±1.8	250	5.6
191105_2a_II	273±10	11.7±2.1	240	6.1
191105_2a_III	254±9	8.1±1.9	240	5.8
191105_3a_I	278±4	16.7±2.5	215	6.7

[1] Horizontal LINET stroke distributions with a high temporal resolution (10 min) were used to determine the mean motion of a thunderstorm cell (V_s).

Table 6. Representativeness of the selected SCOUT-O3 penetrations: estimates of the mean NO/NO_y ratio, mean age of the lightning emissions, mean distance from the lightning activity and from the mean cloud top height.

Flight and Anvil Penetration/tropical (t), subtropical (s) or Hector (H)	Mean NO/NO_y ratio	Estimated mean age of lightning emissions, minutes	Estimated mean distance from lightning activity, km	Mean distance from mean cloud top height, km
191105_1a_I (t)	0.83	30–60	20–40	0.6
191105_2a_x (t)	0.67	15–45	10–30	3.4
191105_2a_I (H)	0.78	15–45	20–40	1.4
191105_2a_II (H)	0.78	30–60	10–30	1.1
191105_2a_III (H)	0.75	90–120	30–50	1.1
191105_3a_I (s)	0.61	60–90	70–90	1.0

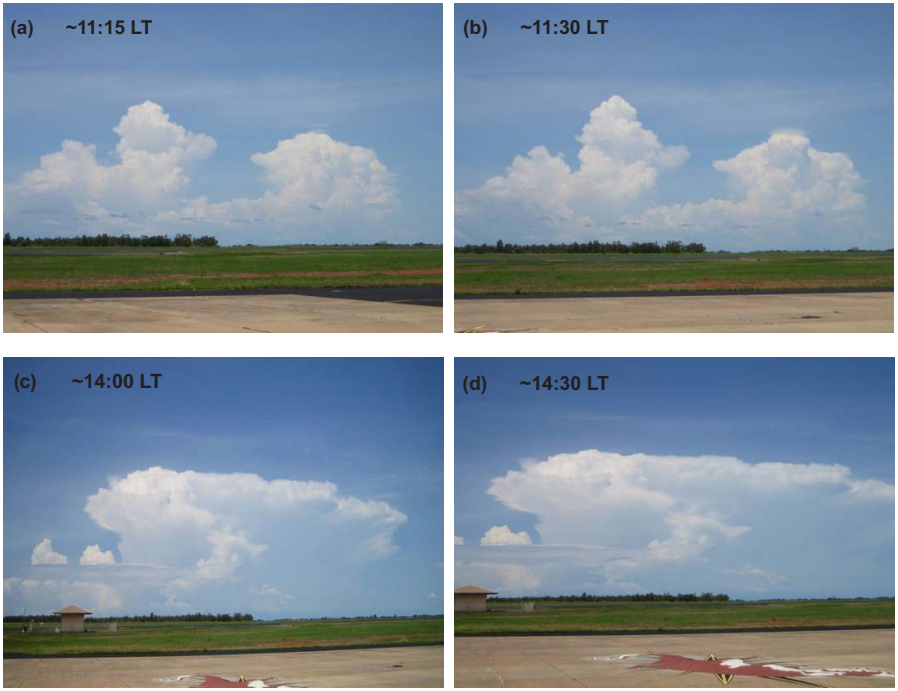

Fig. 1. Photo time series showing the development of the well-known "Hector" thunderstorm over the Tiwi Islands north of Darwin on 30 November 2005 during the SCOUT-O3/ACTIVE field phase (all times given are local time=LT). The merging of several single systems is visible.

ACPD
9, 14361–14451, 2009

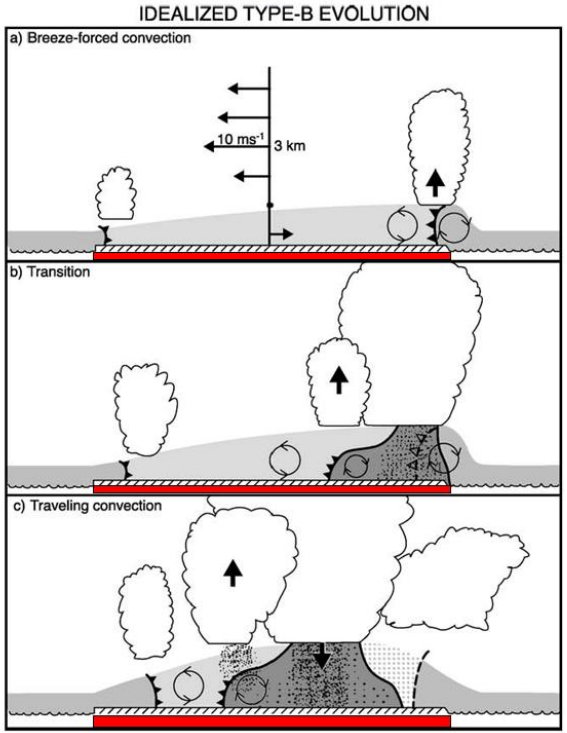

Fig. 2. Schematics of an idealised Hector type B evolution over the Tiwi Islands (red) in E–W cross section during the different development stages **(a–c)**. In addition in (a) the typical westerly surface flow and easterly shear above is shown. Grey shaded areas indicate BLs and cold pools where the darkness is suggestive of coolness and precipitation is speckled. The hatched area to the rear of the mature cold pool in (c) is a recovering island BL after the convective interception of the original sea breeze front. The schematics are not according to scale (adapted from Carbone et al., 2000).

ACPD
9, 14361–14451, 2009

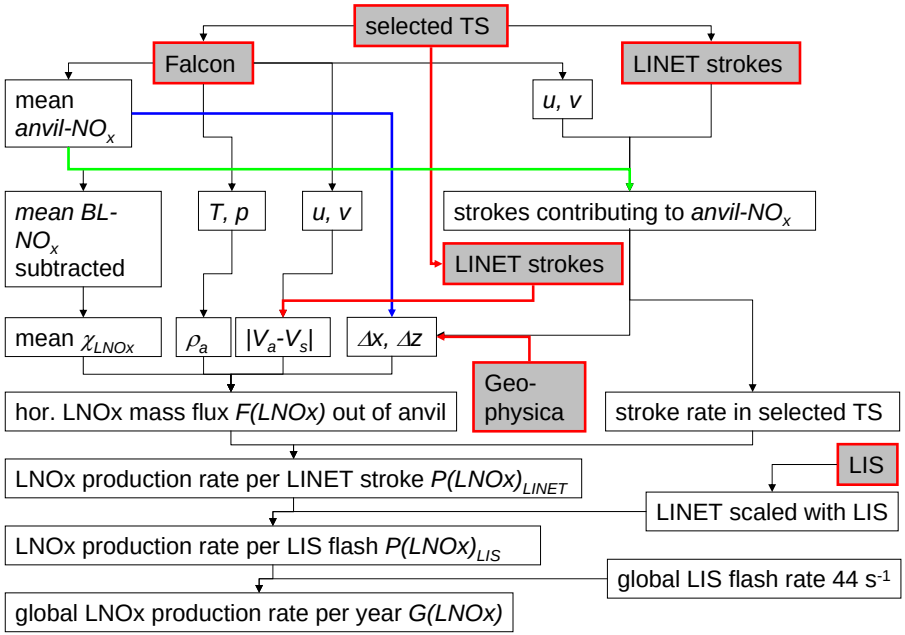

Fig. 3. Flow chart showing the introduced method to estimate the annual global LNO_x production rate from SCOUT-O3 field measurements (Falcon, Geophysica, LINET) combined with LIS data of the selected thunderstorms (TS) all indicated with grey background. Different line colours are used to avoid misunderstanding of the flow direction at line intersections (adopted from HH08 and slightly modified).

ACPD
9, 14361–14451, 2009

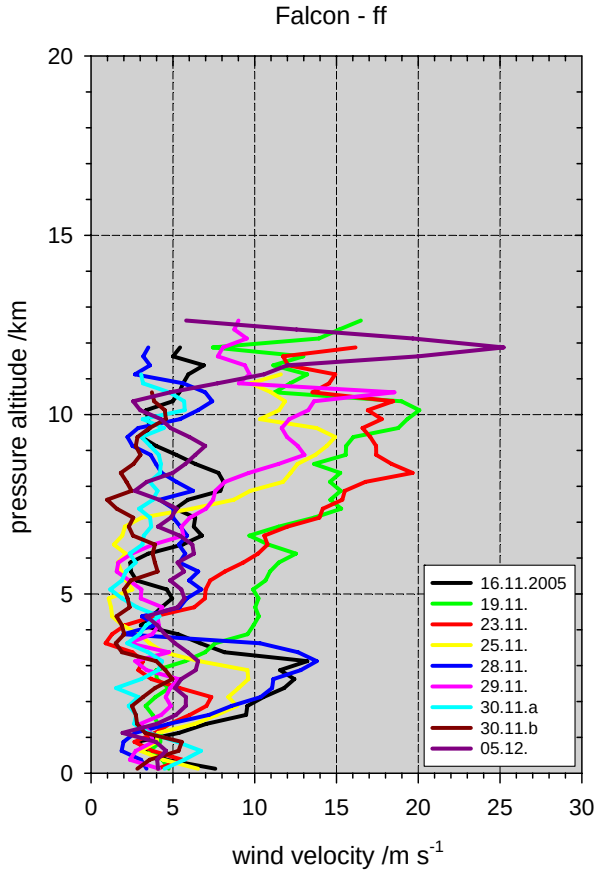

Fig. 4. Mean vertical profiles of the horizontal wind velocity (ff) derived from measurements with the Falcon aircraft. Mean values for every 250 m altitude bin are given for all available SCOUT-O3 flights (dd:mm:(yyyy)) in colour.

ACPD
9, 14361–14451, 2009

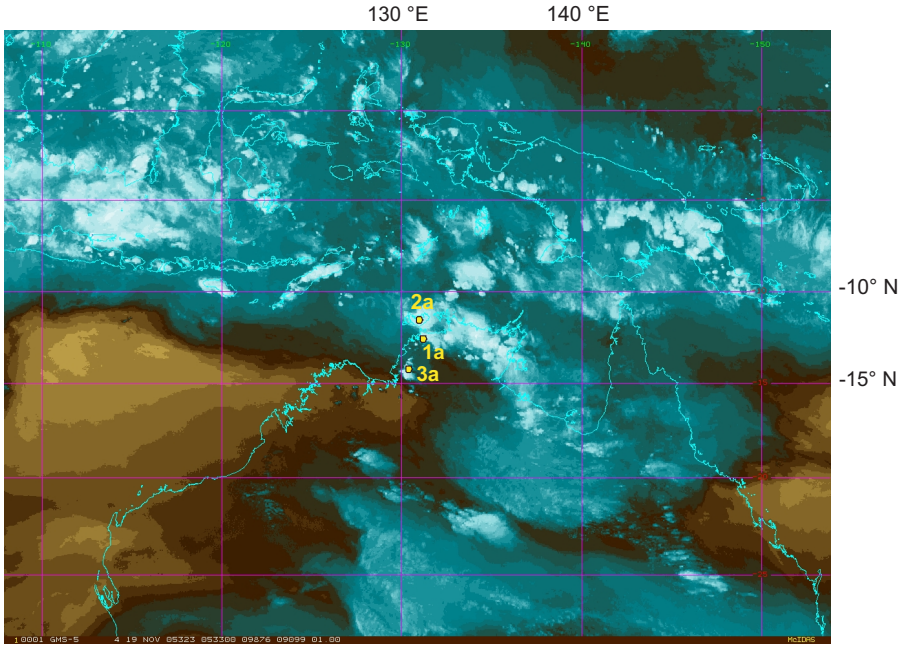

Fig. 5. WV-image (GMS-5) from 19 November 2005 at 05:33 UTC showing the cloud distribution over northern Australia and Indonesia. A sharp transition zone between moist (tropical) airmasses in the vicinity of Darwin (−12.4° N, 130.9° E) and further north (blue colours), and more dry (subtropical) airmasses ∼200–300 km south of Darwin (brown colours) is also clearly visible. Selected thunderstorms probed by the aircraft are labelled in yellow: "1a" close to Darwin (tropical airmass over continent"), "2a" Hector over the Tiwi Islands (tropical maritime continent), and "3a" further to the south of Darwin (subtropical airmass over continent).

ACPD
9, 14361–14451, 2009

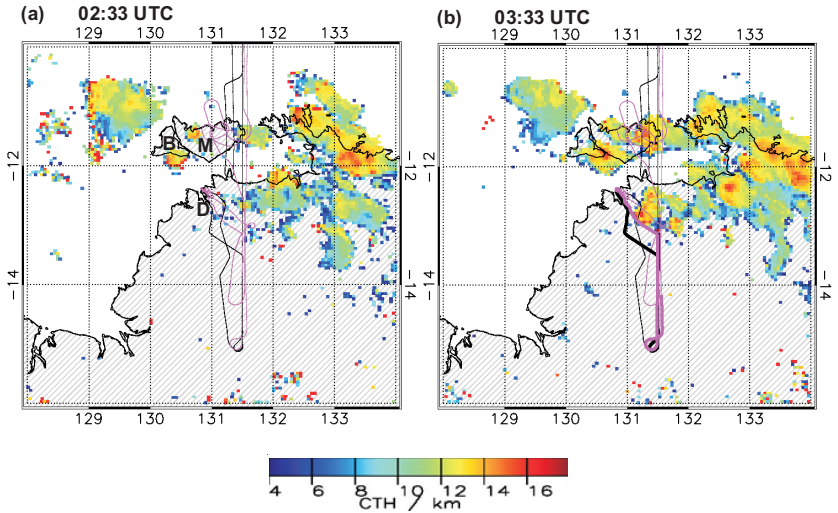

Fig. 6. Hourly maps showing the cloud top height (CTH) distribution based on MTSAT-1R data over northern Australia on 19 November 2005 for the time period 02:33–07:33 UTC **(a–f)**. Superimposed are the flight tracks from the Falcon (black) and Geophysica (dark pink) aircraft. The flight track corresponding to the time between image and +1 h is bold. Darwin is indicated with "D" and the two Tiwi Islands are indicated with "M" for Melville (eastern island) and "B" for Bathurst (western island) in (a) in black. Selected thunderstorms probed by the aircraft are labelled in (c) in black: "1a" close to Darwin, "2a" Hector over the Tiwi Islands, and "3a" further to the south of Darwin.

ACPD
9, 14361–14451, 2009

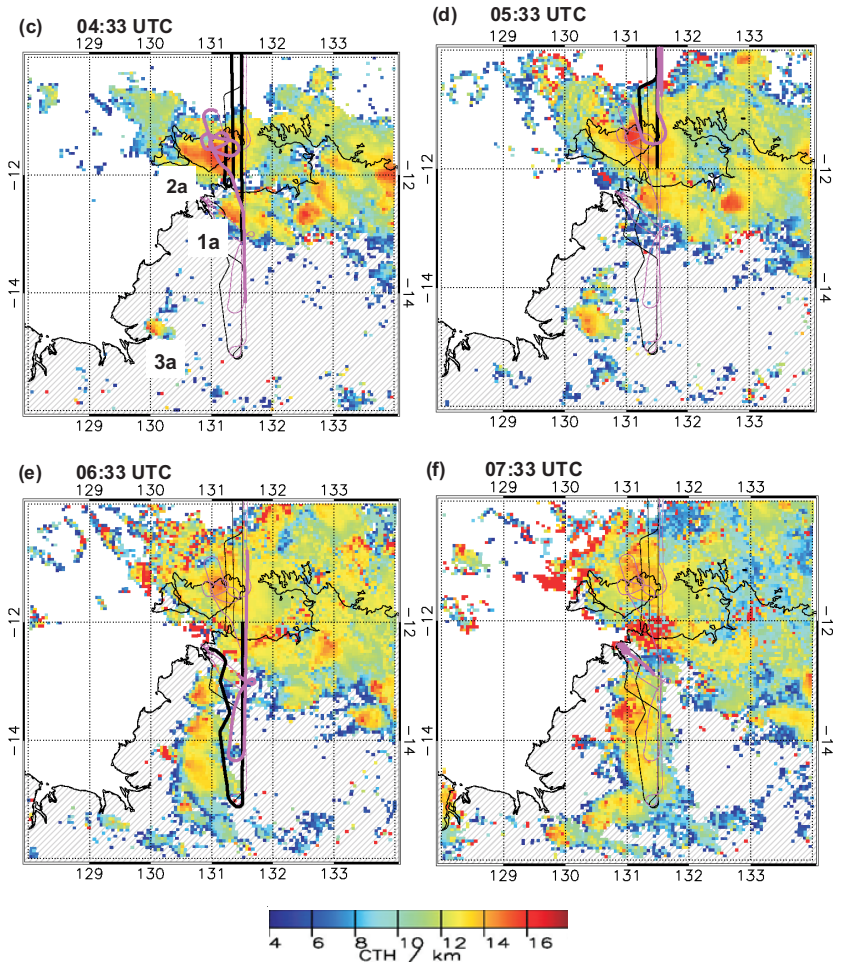

Fig. 6. Continued.

ACPD
9, 14361–14451, 2009

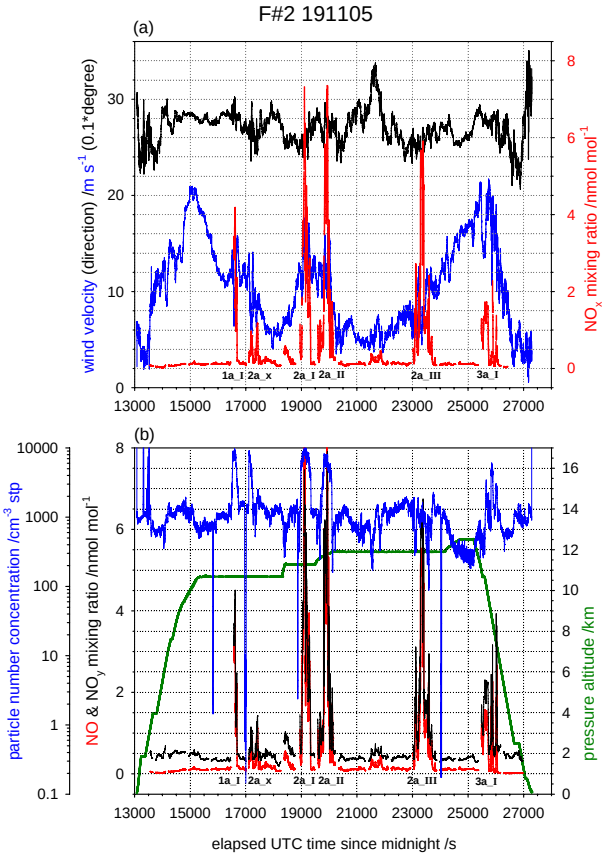

Fig. 7. Time series of NO_x, wind velocity and direction in **(a)** and NO, NO_y, CN, and pressure altitude in **(b)** for the Falcon flight on 19 November 2005. Anvil penetrations are labelled in black.

ACPD
9, 14361–14451, 2009

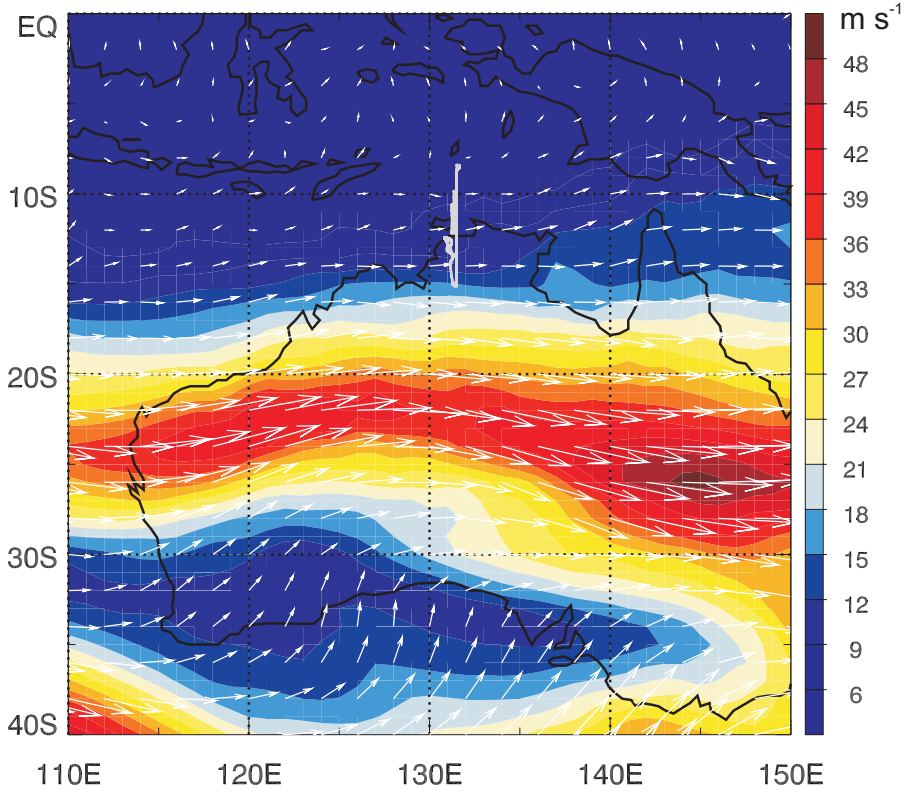

Fig. 8. ECMWF analysis for the wind velocity (in colour) and direction (white arrows) at the 200 hPa level (~12 km, anvil outflow) for 19 November 2005 at 06:00 UTC. The Falcon flight track over northern Australia is indicated in white.

ACPD
9, 14361–14451, 2009

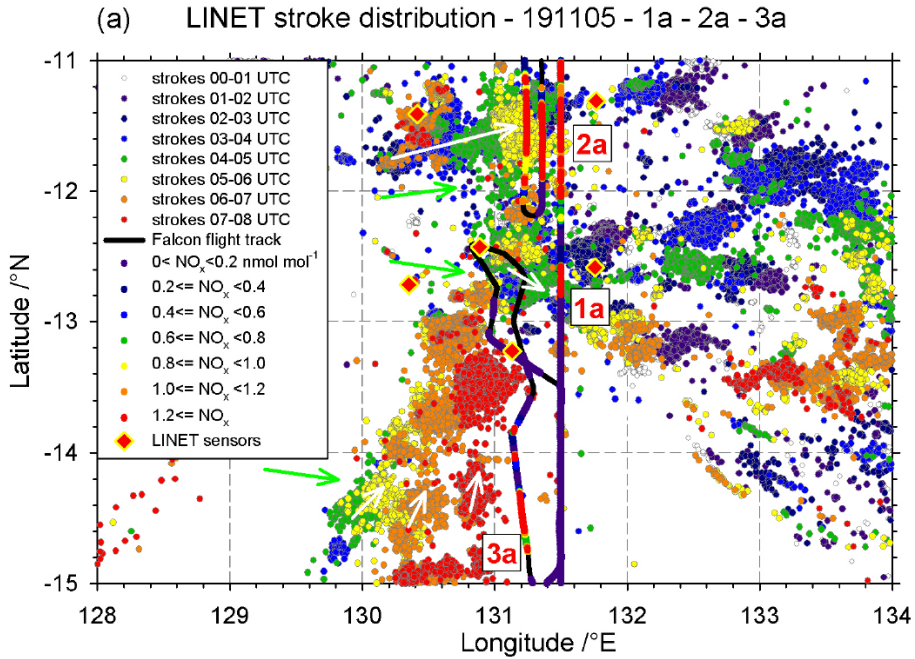

Fig. 9a. Spatial and temporal LINET stroke distribution on 19 November 2005 between 00:00 and 08:00 UTC (upper colour scale). The observed NO_x mixing ratio along the Falcon flight path is superimposed (lower colour scale). Enhanced NO_x mixing ratios were observed during the passage of the anvil outflow of thunderstorms with lightning activity labelled "1a", "2a", and "3a" in **(a)**. All strokes registered before the Falcon penetrated the selected thunderstorm systems "1a", "2a", and "3a" are coloured in **(b)**, **(c)**, and **(d)**, respectively. The white arrows indicate the direction of the storm motion and the green arrows the main wind direction in the anvil outflow (not scaled according to velocity). In addition, the positions of the LINET sensors are indicated (diamonds).

ACPD
9, 14361–14451, 2009

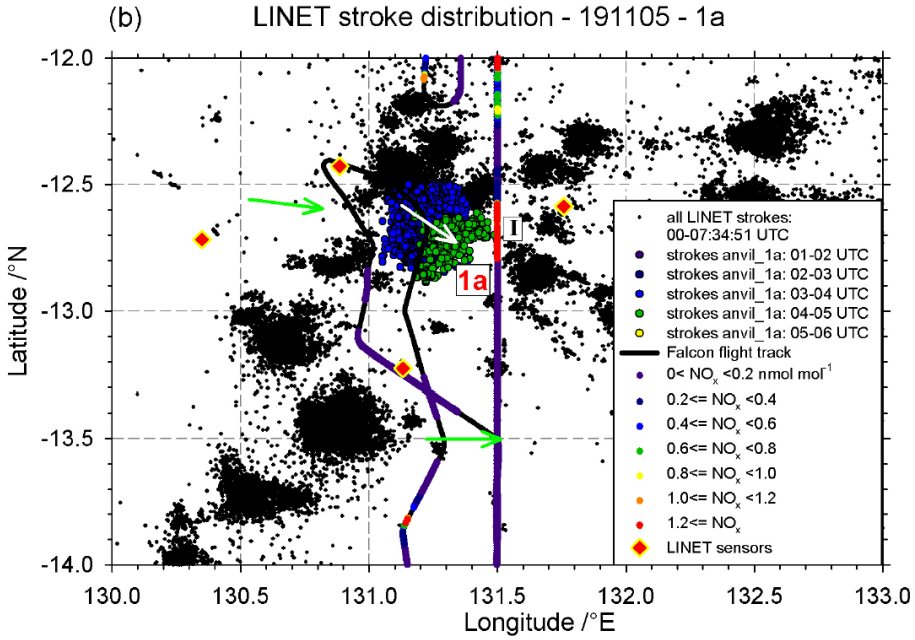

Fig. 9b. Continued.

ACPD
9, 14361–14451, 2009

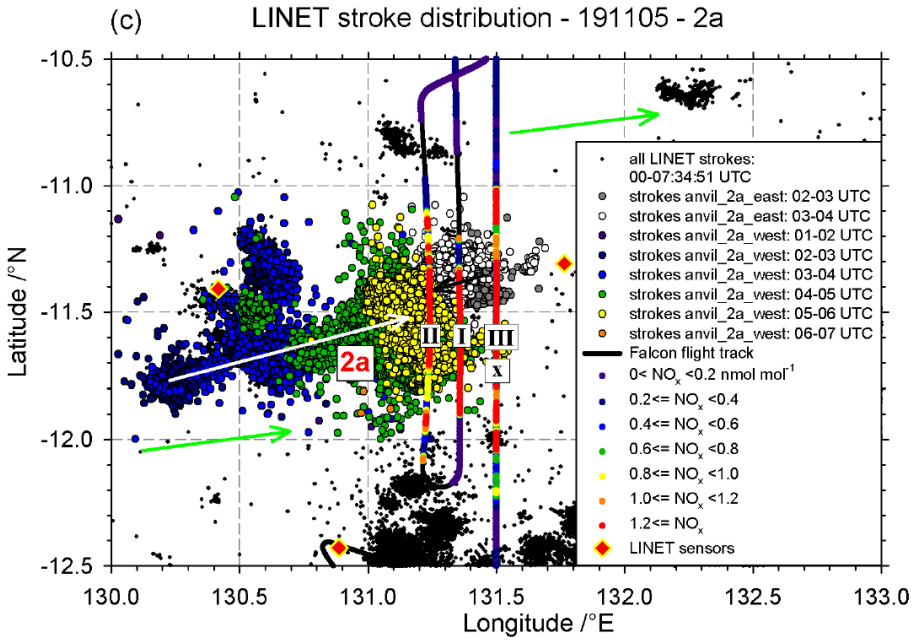

Fig. 9c. Continued.

ACPD
9, 14361–14451, 2009

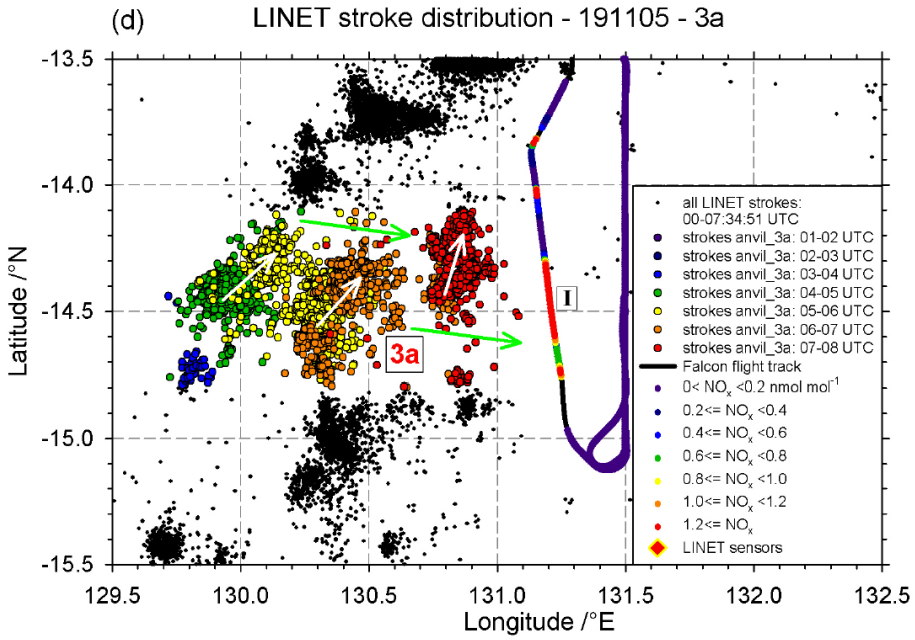

Fig. 9d. Continued.

ACPD
9, 14361–14451, 2009

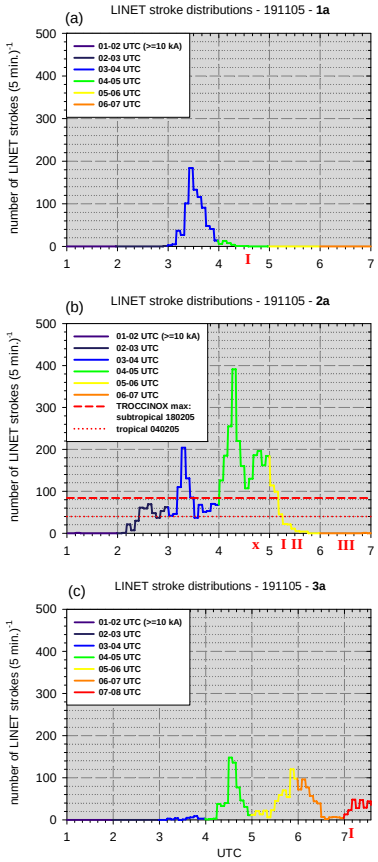

Fig. 10. Time series of LINET stroke rates (colour-coded as in Fig. 9) determined for the selected thunderstorm systems on 19 November 2005 labelled "1a" **(a)**, "2a" **(b)**, and "3a" **(c)** (only strokes with peak currents ≥10 kA considered). The times when the different anvil penetrations took place are labelled in red below the time scale.

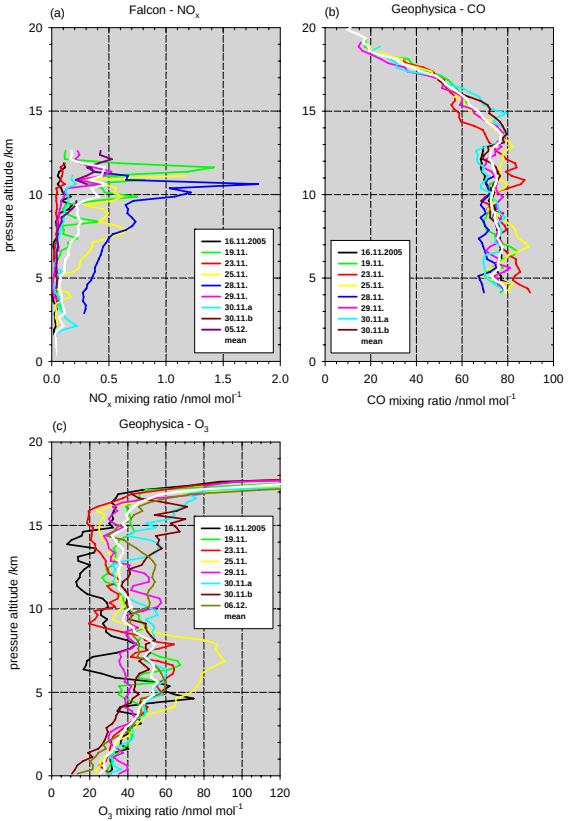

Fig. 11. Mean vertical profiles for NO_x **(a)**, CO **(b)**, and O_3 **(c)** derived from measurements with the Falcon and Geophysica aircraft. Mean values for every 250 m altitude bin are given for all available SCOUT-O3 flights (dd:mm:(yyyy)) in colour. The white lines show the mean of all coloured flight profiles in each figure.

ACPD
9, 14361–14451, 2009

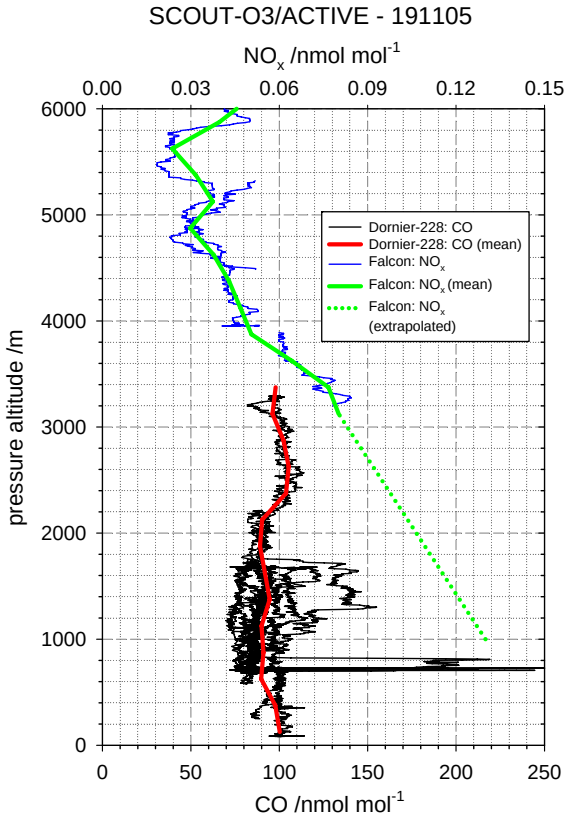

Fig. 12. Vertical NO_x and CO profiles derived from measurements with the Falcon and Dornier-228 aircraft on 19 November 2005. Mean values are given for every 250 m altitude bin (bold lines). An extrapolation of the measured NO_x mixing ratios down to 1 km is indicated by the dotted line.

ACPD
9, 14361–14451, 2009

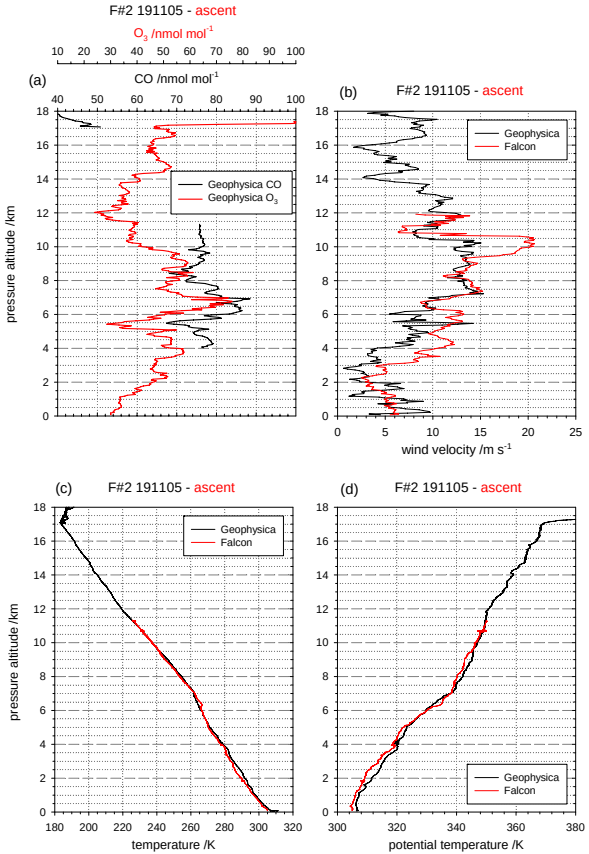

Fig. 13. Vertical profiles for CO and O_3 **(a)**, wind velocity **(b)**, temperature **(c)**, and potential temperature **(d)** derived from measurements with the Falcon and Geophysica aircraft during ascent on 19 November 2005.

ACPD
9, 14361–14451, 2009

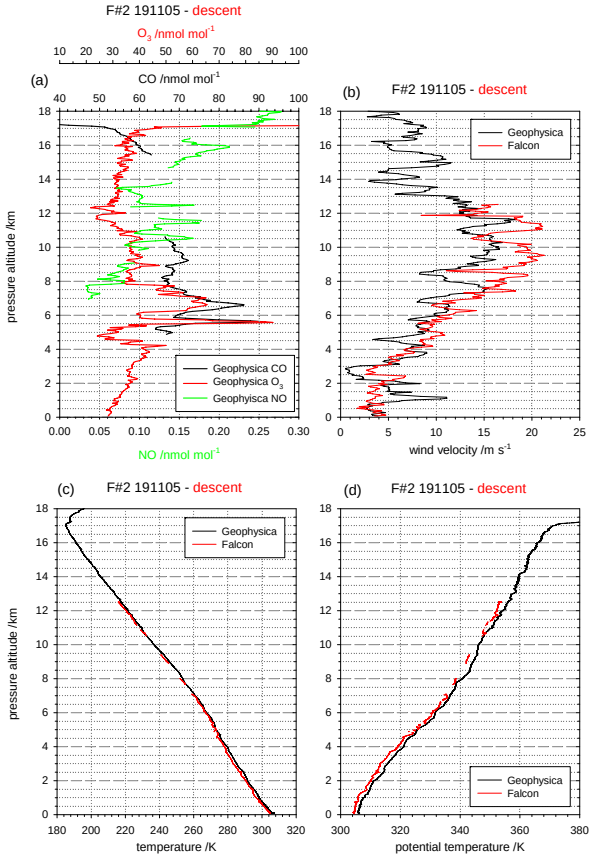

Fig. 14. Vertical profiles for CO, O_3, and NO **(a)**, wind velocity **(b)**, temperature **(c)**, and potential temperature **(d)** derived from measurements with the Falcon and Geophysica aircraft during descent on 19 November 2005.

ACPD
9, 14361–14451, 2009

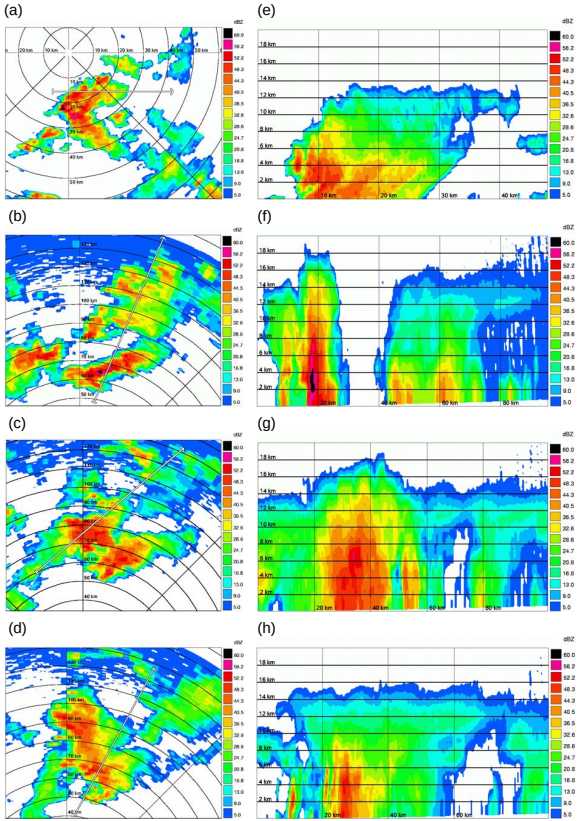

Fig. 15. Horizontal distribution of radar reflectivity **(a–d)** and the corresponding vertical cross-sections **(e–h)** along the white arrows indicated in (a–d) for the 19 November 2005 measured with the CPOL radar in Darwin. In (a) the focus is on thunderstorm "1a" at 04:30 UTC, in (b–d) the focus is on Hector pre-storm developments "2a_x" and the mature and dissipating Hector "2a_I-III" at 04:00 (b), 04:30 (c) and 05:00 (d) UTC.

ACPD

9, 14361–14451, 2009

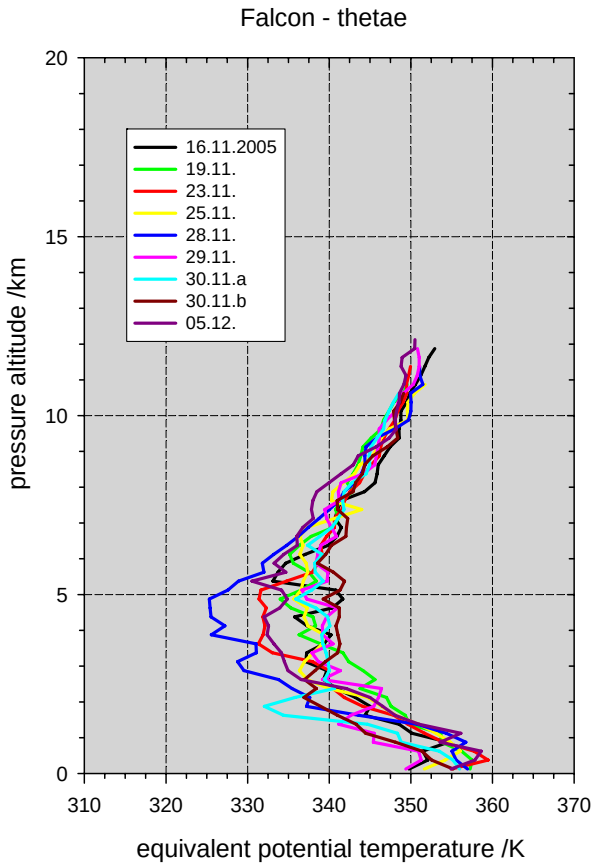

Fig. 16. Mean vertical profiles for the equivalent potential temperature (Θ_e) derived from measurements with the Falcon aircraft. Mean values for every 250 m altitude bin are given for all available SCOUT-O3 flights (dd:mm:(yyyy)) in colour.

ACPD
9, 14361–14451, 2009

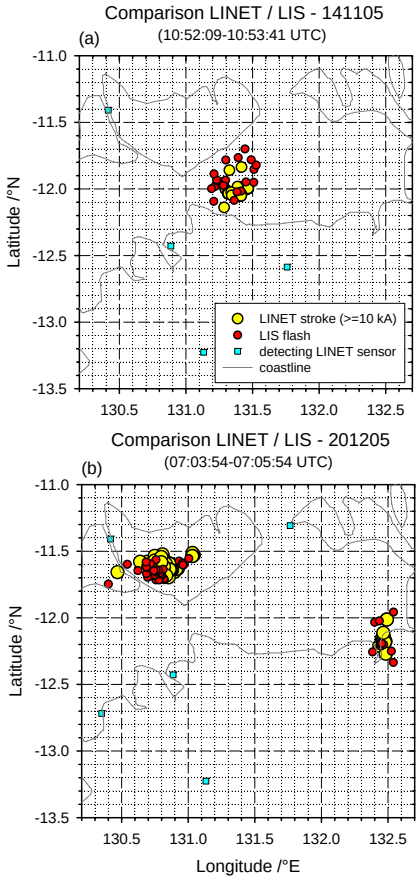

Fig. 17. Horizontal distributions of LIS flashes (in red) and LINET strokes with peak currents ≥10 kA (in yellow) during the LIS overpass over the LINET area on 14 November **(a)** and 20 December 2005 **(b)**. Detecting LINET sensors are superimposed (in cyan).

ACPD
9, 14361–14451, 2009

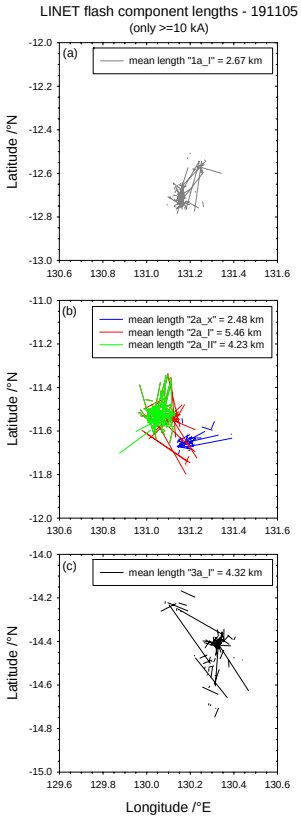

Fig. 18. Horizontal distributions of LINET flash component lengths (several close-by VLF/LF sources in time and space connected to a line) for the selected Falcon penetrations "1a_I", "2a_x", "2a_I", "2a_II" and "3a_I" of the anvil outflow from thunderstorms with lightning activity on 19 November 2005. The lengths given are mean LINET flash component lengths determined during 20 min, when the stroke activity contributing to observed LNO_x peaked.

ACPD
9, 14361–14451, 2009

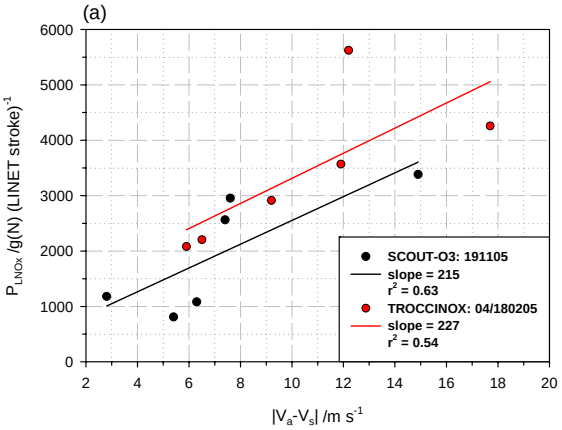

Fig. 19. Correlation between the vertical wind shear $v_a - v_s$ (between the anvil outflow and the steering level) and the LNO_x production rates P_{LNO_x} **(a)** and G_{LNO_x} **(b)** for selected SCOUT-O3 and TROCCINOX thunderstorms (labelled in (b) and **(c)**. Different LINET/LIS factors where used in (b): 1.6 for SCOUT-O3 and 0.5 for TROCCINOX. In (c) the correlation between the flash component length and the width Δx of the anvil outflow perpendicular to the wind direction is shown.

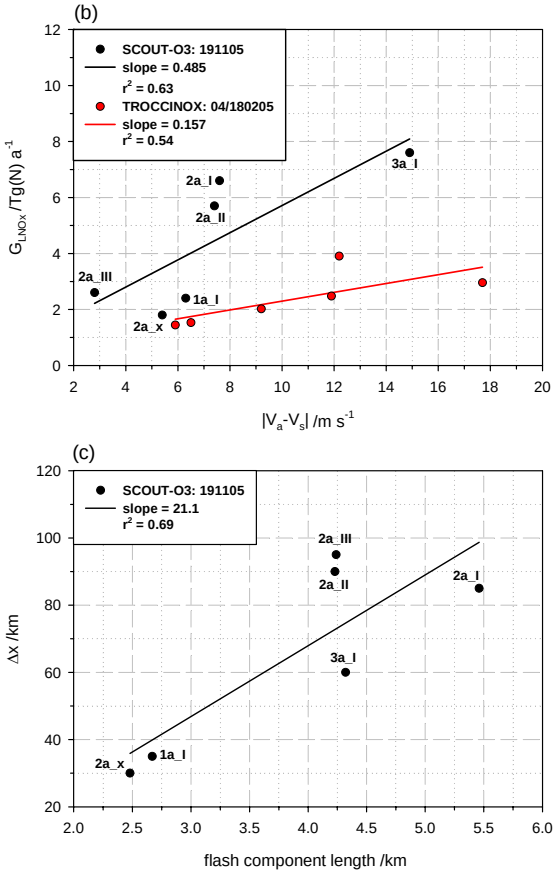

Fig. 19. Continued.

ACPD
9, 14361–14451, 2009

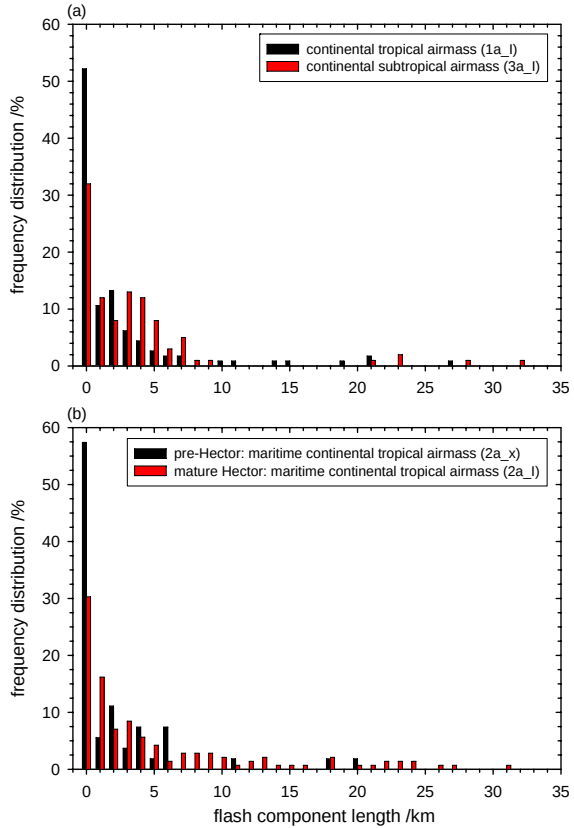

Fig. 20. Frequency distributions of LINET flash component lengths on 19 November 2005 for thunderstorm "1a_l" and "3a_l" **(a)** and for thunderstorm "2a_x" and "2a_l" **(b)**. For a given flash component length of e.g. "1 km", all lengths between ≥1.0 and <2.0 km were summarised.